DESIGN, PERFORMANCE PREDICTION AND VALIDATION OF A SEED ORIENTING CORN PLANTER

By

ADRIAN ALOIS KOLLER

Bachelor of Science in Aerospace Engineering
University of Michigan
Ann Arbor, MI
2002

Master of Science in Aerospace Engineering
Georgia Institute of Technology
Atlanta, GA
2005

Submitted to the Faculty of the
Graduate College of the
Oklahoma State University
in partial fulfillment of
the requirements for
the Degree of
DOCTOR OF PHILOSOPHY
May, 2013

DESIGN, PERFORMANCE PREDICTION

AND VALIDATION OF A SEED ORIENTING

CORN PLANTER

Dissertation Approved:

Dr. Michael D. Buser

Dissertation Adviser

Dr. Randal K. Taylor

Dr. Paul R. Weckler

Dr. William R. Raun

ACKNOWLEDGEMENTS

First and foremost, I would like to thank my advisor Dr. Michael Buser and my committee members Dr. William Raun, Dr. Randy Taylor and Dr. Paul Weckler. Their mentoring and the time they took for countless discussions have made this work possible in the first place. I truly appreciate the support and leeway they have given me throughout the pursuit of this novel and rather unconventional research topic. My gratitude also goes towards Dr. Marvin Stone and Dr. John Solie whose feedback has been invaluable at many occasions.

My research teammates Elizabeth Miller, Wesley Porter, and Jorgé Rascón were always there with a helping hand and data collection in the lab, the greenhouse and the field was supported by our junior team members Brian Biggerstaff, Staci Cuccio, Kevin Roewe, Jace Reed, and Andrew Slavens. My "cubicle mate" Erin Daley always managed to keep the supply of fun and motivation high. Thanks y'all.

Implementation of the design was supported by the Biosystems Engineering Shop, run by Mr. Wayne Kiner and Mr. Nick "Shorty" Sempter. Without their feedback on my drawings this planter would not have been built.

I would like to thank also Dr. Guilherme Torres whose parallel research on the agronomic aspects of seed orientation has led to many joint hours in the field and innumerable debates on the topic.

My stay in Oklahoma was rendered unforgettable also by the Dicks Family, who has "adopted" me as one of their own. Ellen, Mike, Shane, Tina, Evan, Jake, and Maggie, I truly enjoyed my time on the Cimarron Dunes Farm.

Equal gratitude is deserved by my family, especially my parents Lydia and Alois for their unconditional support. Special thanks goes to my Dad who supported some of the final data collection and image analysis once back in Switzerland.

However, my deepest appreciation and thankfulness is deserved by my partner Cornelia Stüssi who has tolerated me leaving for two years and spending uncountable nights and weekends working on the completion of this work.

My dissertation is dedicated to my buddy Nimrod – too many jokes remain untold without you.

Name: ADRIAN ALOIS KOLLER

Date of Degree: MAY, 2013

Title of Study: DESIGN, PERFORMANCE PREDICTION AND VALIDATION OF A SEED ORIENTING CORN PLANTER

Major Field: BIOSYSTEMS ENGINEERING

Abstract:

Investigations into active control of corn canopy architecture through manipulation of seed orientation at planting have shown that specific seed orientations produce highly aligned leaf azimuths. Data obtained from hand planted field trials with across-row oriented leaves show that such canopies intercept more light and ultimately produce higher yields.

This study was conducted to investigate the feasibility of mechanized seed orientation through the concept of part orientation by pushing. 3D-scans of 15 "medium flat" kernels of the hybrids DKC-6342, DKC-6346, P0902HR and P1162HR have been computationally analyzed to determine stable seed orientations when subjected to pushing. These predicted results were compared to data obtained in bench tests. The concept was then refined and integrated into a prototype planter based on a standard off-the-shelf row unit. The prototype was first tested in a soil bin at laboratory conditions and then in the field. Because field tests do not allow measurement of seed orientations directly greenhouse studies of the relationship between seed orientation and seed leaf azimuth distributions were conducted to assess the feasibility of an indirect post-emergence performance measure.

The computational model was able to predict seed orientation by pushing very accurately. The analysis and subsequent bench unit and prototype tests revealed that orientation performance is dependent on seed shape with the kernels of DKC-6342 being the most and those of P1162HR the least suitable. Soil bin and field data confirmed that at least parity between seed and ground velocity must be achieved in order to maintain orientation during transition from the orientation mechanism to the ground. The greenhouse studies led to the conclusion that seed-to-leaf azimuth distributions can be described by von Mises models. Due to the specific design of the orienter, the shape of the kernels, and the observed seed-to-leaf azimuth properties the measureable seed leaf azimuth distribution in the field is expected to be a von Mises mixture containing four modes. The complexity of such a mixture inhibits the accurate, indirect determination of seed orientation performance in the field.

TABLE OF CONTENTS

LIST OF TABLES

LIST OF FIGURES

CHAPTER I

INTRODUCTION

The Effect of Seed Orientation on Corn Plant Morphology

Corn (Zea mays l.) is one of the most prevalent plants cultivated for food and feed production worldwide. In 2008 corn grain production exceeded 800 million metric tons and has since grown to 850 million tons in 2012, despite a year with severely lower yields due to drought conditions in much of the United States (USDA-FAS, 2012b). Continued improvement in genetic selection and agricultural practices have managed to increased corn grain yields at roughly 120 kg(ha yr)$^{-1}$ more than nine fold to more than 9 tons per hectare over the past 80 years (USDA-FAS, 2012a).

Corn Yield and the Canopy Architecture

Plant leaves are exposed to the incident sunlight and function as the critical energy input channel (Stewart et al., 2003) into the plant and drive the plant organ development (Maddonni and Otegui, 1996). In addition, the leaves shade the ground and may reduce evaporative water loss and make it more difficult for weeds to prosper (Singer et al., 2000; Tollenaar et al., 1994).

The importance of canopy architecture, that is the spatial arrangement of the leaves in a plant community, has been under investigation for some time. Loomis and Williams (1969) and Blad and Baker (1972) examined leaf azimuth distributions of corn and soybean stands and found evidence that light interception efficiency is the primary factor determining grain yield under the condition that all other critical factors (genetic potential, available soil moisture, nutrient supply, air temperature, etc.) are not limiting (Pendleton and Peters, 1967). Gardner et al. (1985) detailed

how leaf area strongly influences the light interception characteristics and discovered that it determines dry matter accumulation and the resulting yield. Girardin (1992) and Girardin and Tollenaar (1994) examined leaf azimuth distributions in corn canopies and found a non-uniform distribution attributable to intraspecific interference and competition for light. These findings were later reinforced by research conducted by Fortin and Pierce (1996) and Maddonni et al. (2002). Other research suggested that the non-uniform randomness may also partially be attributed to wind effects or row orientation with respect to the solar path (Elmore et al., 2005).

Corn plants are generally distichous plants (Paliwal et al., 2000) and arrange their leaves roughly in a plane alternatingly on opposite sides of the stalk. Andrieu et al. (1995) developed astoundingly realistic leaf distribution and light interception models based on three-dimensional canopy scans. Maddonni et al. (2002) showed that some hybrids have the ability to react to intraspecific interference and mutual shading by reorienting their newly emerging leaves several degrees during the first few growth days such that they occupy the unobstructed spaces in the canopy. This research led to a much better understanding of the plant-to-plant interaction dynamics and the development of higher-fidelity simulation models (Chelle et al., 2004; Lopez-Lozano et al., 2007).

Higher Light Interception Means Higher Yield

Toler et al. (1999) examined the effects of leaf orientation on light interception and yield and first documented higher light interception and yield for plots with oriented leaves. Maddonni et al. (2001) came to similar conclusions earlier when he looked at canopy efficiency with simulations and light interception measurements in the field. Investigations on hand-planted plots conducted by Torres (2012) reiterate on some of the work by Toler et al.. The data provides evidence that plots with across-row oriented leaf azimuths significantly enhance the yield potential by 9 to 14% over randomly oriented seeds, and a reduced plant-by-plant yield variability.

The fraction of incident photosynthetically active radiation (fIPAR) absorbed by the canopy is a commonly accepted measure (Maddonni and Otegui, 1996) of a canopy's ability to absorb sunlight. Figure 1 depicts a typical relationship between leaf area index (LAI = total leaf area per surface area of soil) and fIPAR. As indicated in the figure, an oriented canopy is expected to exhibit higher light interception efficiency at a given LAI (Torres, 2012). Consequentially, canopy closure can be achieved faster which has been shown to generate a number of beneficial secondary effects like improved repression of weeds, reduced evaporation, etc. (Westgate et al., 1997).

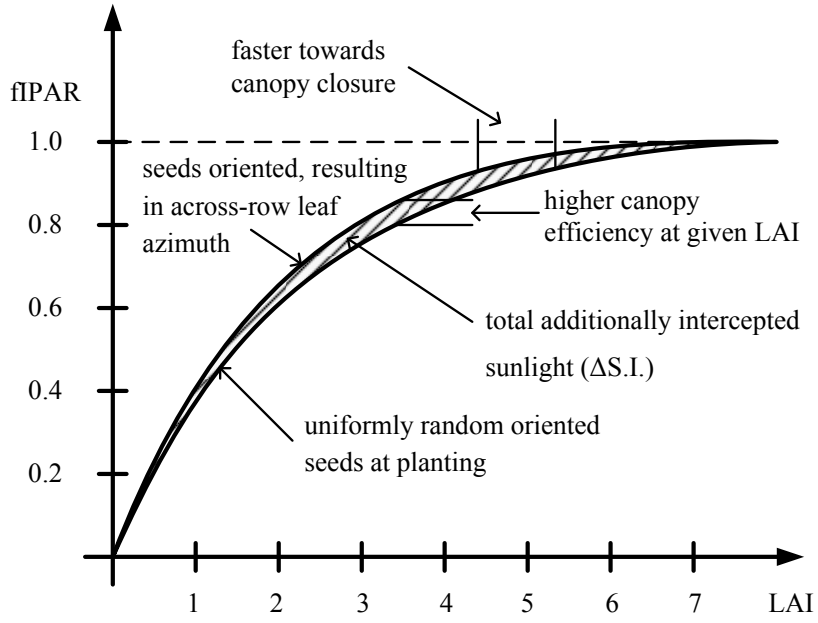

Figure 1. Qualitative relationship between leaf area index (LAI) and fraction of incident photosynthetically active radiation (fIPAR) for canopies with randomly oriented and across-row oriented leaf azimuths.

The total additionally intercepted sunlight (ΔS.I.) during the growth period, the shaded area in Figure 1, is then a function of the ability to control the leaf azimuth distribution. The more

precisely the leaf azimuths can be aligned and prevented from overlapping, the higher the expected additionally intercepted sunlight.

The relationship between additionally intercepted sunlight and leaf azimuth distribution is currently unknown. Figure 2 depicts three such hypothetical relationships. Curve 1 represents an interaction that shows a lot of improvement with respect to ΔS.I. for only a slight improvement in leaf azimuth alignment. This constitutes an ideal case, meaning that with minimal improvement of leaf azimuth alignment, the benefits would already manifest itself. Curve 3 on the other hand represents a major challenge because the required leaf azimuth alignment must be very accurate in order to produce a significant improvement in sunlight interception performance.

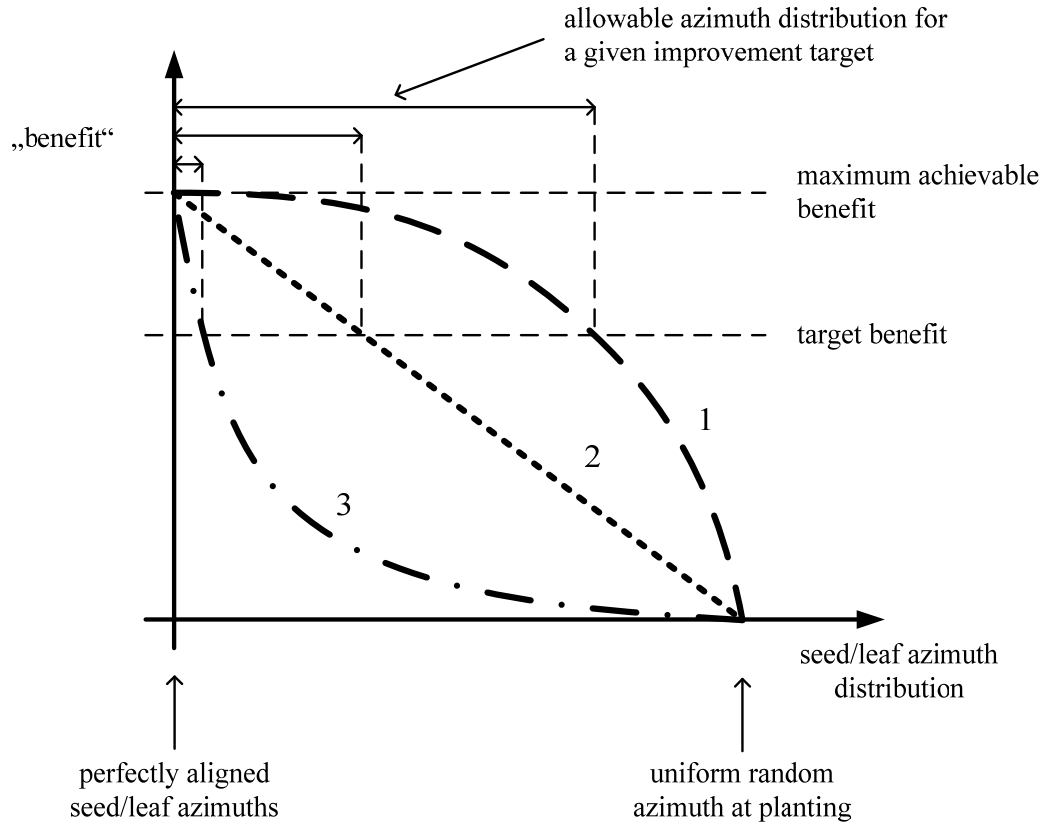

Figure 2. The relationship between additionally intercepted sunlight and seed or leaf azimuth distribution is currently unknown.

How Seed Orientation Influences Canopy Architecture

The azimuth orientation of the vertical leaf plane in which the distichously arranged leaves lie depends on the initial seed orientation. Peters and Woolley (1959) first mentioned in "Agricultural Research" that if the seeds are arranged in a specific orientation at planting, the plants would grow such that the leaves point preferentially into the space between the rows. Peters and Woolley noticed that kernels planted "points down and flat sides running with row … brings leaves out almost at right angles to the flat side of the kernel" (Figure 3). Fortin and Pierce (1996) investigated the azimuth angle of ear leaves with respect to seed orientation and Toler et al. (1999) conducted field experiments to assess the impact of light interception on yield based on hand-planted trials with across-row oriented leaves. Toler et al. found evidence similar to the observations by Peters and Woolley for significantly higher yields for plots with across-row oriented leaf azimuths.

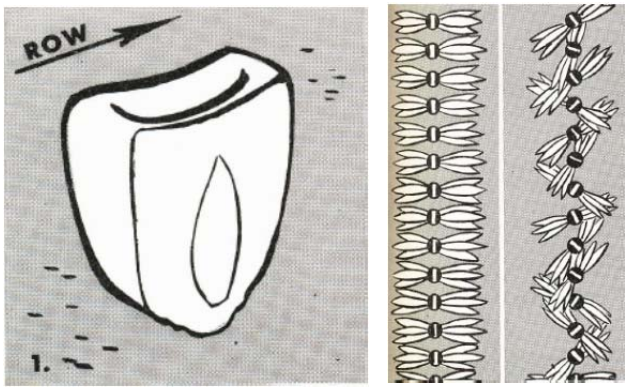

Figure 3. The effect of seed orientation on leaf azimuth distribution was documented as early as the late 1950s. Figure from Peters and Woolley (1959). Seeds planted upright with the caryopsis attachment point down and the embryo across the row as shown in a) produces preferentially across-row oriented leaves as shown in b). Random seed orientation produces randomly orientated leaf azimuths as depicted in c).

Torres et al. (2011) systematically examined the effect of seed orientation on leaf azimuth distribution and showed that three seed orientations produce preferentially across-row oriented leaves. Confirming the findings by Peters and Woolley (1959) and Toler et al. (1999), Torres et al. showed that orienting the seed upright with the caryopsis attachment point down and embryo facing across the row produces preferentially across the row oriented leaves. However, as depicted in Figure 4, Torres et al. also showed that laying the seed flat with the embryo either up or down and the caryopsis attachment point across the row would produces similar results.

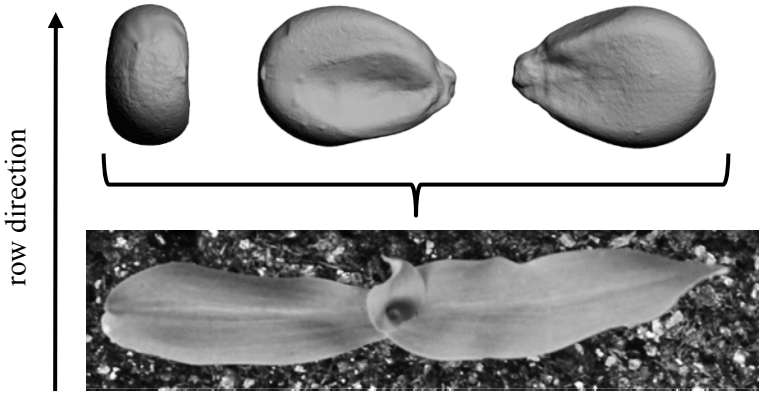

Figure 4. Torres et al. (2011) found three seed orientations produce preferentially across the row oriented leaves.

The fact that leaf azimuth distribution can be influenced by seed orientation relates back to Figure 2: the degree of accuracy to which seeds can be oriented determines the amount of additionally intercepted light and hence, the yield advantage. Hand-planted experiments likely produce leaf azimuth distributions which are fairly accurate. To determine the shape of the relationship depicted in Figure 2, various planting methods, preferably mechanized, should be investigated more closely. Orientation uniformity achieved by hand-planting may be limited and emergence uniformity is just as important. Differences in quality of seed-soil contact between machine- and hand-planted plots are likely present. A direct yield comparison with respect to planting technologies should therefore involve mechanized planting methods.

Exterior Seed Features and Seed Grading

A corn kernel's shape resembles a falling water drop's elongated form. Figure 5 depicts the prominent exterior features. The caryopsis attachment point is the "tip" where the kernel is attached to the cob. The embryo is located right behind the indentation on the side of the kernel. The pericarp, the shiny hull around the rest of the seed, protects the endosperm which provides the energy reserve for the germination process (Paliwal et al., 2000).

The kernels on an ear, also called a cob, do not all possess the same shape. As depicted in Figure 6, the kernels attached to the cob at both ends tend to take a rounder shape while the kernels in the middle of the cob are flatter.

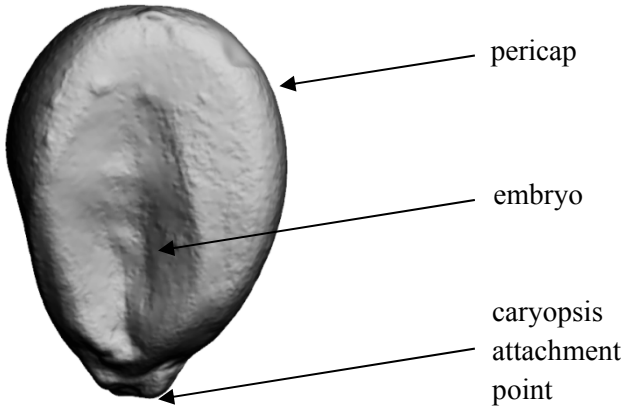

Figure 5. The location of the embryo, the caryopsis attachment point, and the pericap are the prominent exterior features of the corn seed.

Today's precision corn planting equipment is designed to function particularly well with certain types of seed. For that reason, seed companies grade the seed corn and market the shape types accordingly. "Large Flats", "Medium Flats", "Small Rounds" or "Medium Rounds" are common denominations for commercial corn seed grades (Monsanto Imagine, 2008). At the same time, planter manufacturers provide specifically designed exchangeable parts for the equipment so that the farmer may choose the type of seed grade to plant.

While internationally recognized definitions and requirements for genetic purity, germination performance, or seed integrity are well established for seed in general (Code of Federal Regulations, 2012a, b; OECD, 2011), seed shapes or company specific grading schemes are not subject to any such regulatory frameworks.

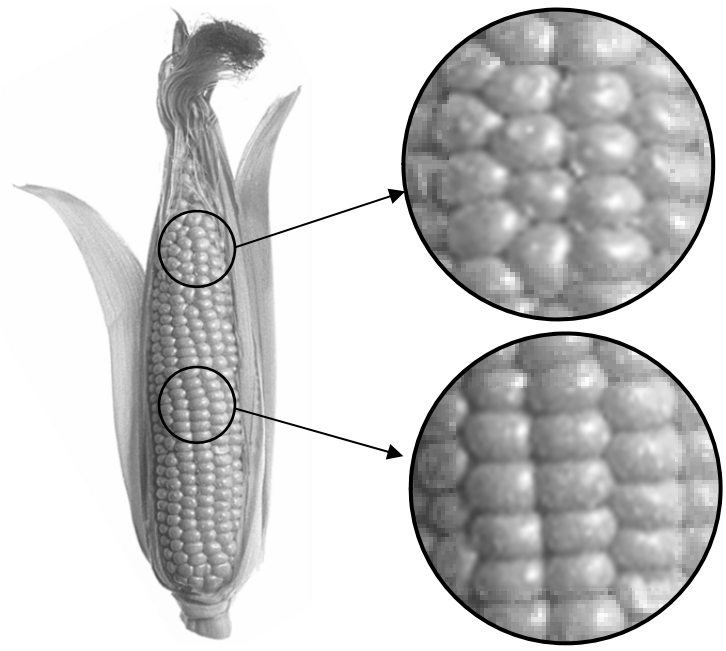

Figure 6. Kernel shape depends on the hybrid and the location on the cob. Kernels at both ends of the cob tend to be round, in the middle of the cob, they take a flatter shape.
Image source: http://www.wpclipart.com.

Despite the grading schemes applied by seed suppliers, the variability across hybrids for even the same grading type is significant. The "large flats" for the Pioneer hybrids P0902HR and P1162HR depicted in Figure 7 look quite differently although they underwent identical grading processes. The P0902HR kernels are narrower at the caryopsis attachment point and resemble more the shape of a falling water drop. The P1162HR large flats are of quite uniform thickness throughout and have a very round, almost discoidal shape.

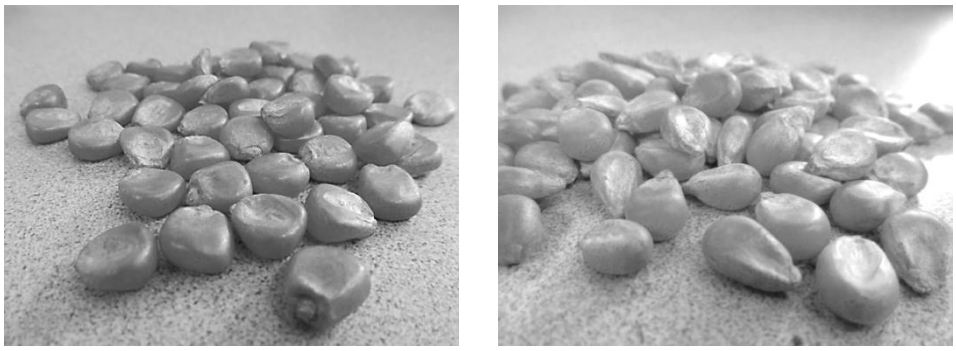

Figure 7. The kernel shape differences between hybrids become apparent when comparing "large flats" for P1162HR (left) and P0902HR (right).

Earlier Concepts for Oriented Planting

Peters and Woolley (1959) suggested in their publication that the "difficulties in mechanical planting of oriented seed corn can be overcome by fastening the kernels to a continuous tape and planting the tape". While this technique has existed for nearly 100 years (McComb, 1915) and is quite commonly applied especially in vegetable production for plants with very small seeds, it is not suitable for today's large-scale corn production. At seeding rates of 60,000 to 100,000 plants per hectare and planting speeds of 8 to 13 km/h (Liu et al., 2004), the logistics of unrolling miles of seed tape 12 to 24 rows at a time would pose a significant challenge.

Citing the publication by Peters and Woolley, Williams (1965) filed a patent for a groove-forming seed orienting planter shoe that would achieve the desired upright seed orientation and proper spatial placement from bulk seed. However, it is unknown whether or not an actual implementation of the concept was ever built.

Research Outline

Detailed investigations into the mechanization aspects of seed orientation are all but inexistent. The overarching objective of this study is therefore to examine the feasibility of one particular

approach and identify the key aspects which may serve as entry points for further research. A conclusive treatment of seed orientation mechanization is not attempted here.

Limitations

While important elements in the determination of the ultimate yield, this research does neither consider seed spacing uniformity nor plant emergence rate. At today's (required) seed vigor (Code of Federal Regulations, 2012a), both spacing uniformity and emergence rate are largely attributable to the planter performance. Nonetheless, seed orienting planting equipment developed for a production environment must achieve similar performance with respect to these measures otherwise a comparison between oriented and random treatments is meaningless. Also, planting speed was not considered in this research. The speeds at which the tests with the subsequently described prototype planter were conducted are in the range of 2 to 3 km/h. This is significantly slower than what can be achieved with currently available equipment (Liu et al., 2004). Hence, all aspects of economic viability of seed oriented planting are at this point irrelevant and left to further research.

Specific Objectives

For this study, the following specific objectives have been formulated:

1) Identify a seed orientation method that can cope robustly with the natural variability among seed corn. Predict the orientation performance by computational analysis of seed corn shapes. Design, build, and test a working model of the orientation concept to validate the computational model through laboratory tests and contrast the predicted and measured performance.
2) Extend the mechanization concept to a prototype implementation that can be tested at planter level at laboratory and field conditions.

3) Through greenhouse studies, assess the feasibility of a post-emergence seed orientation performance measure that allows the indirect determination of seed orientation accuracy in the field.

Research Plan

The research plan depicted in Figure 8 outlines the approach taken in this study. At the same time, this outline provides a graphical overview of the structure of this document.

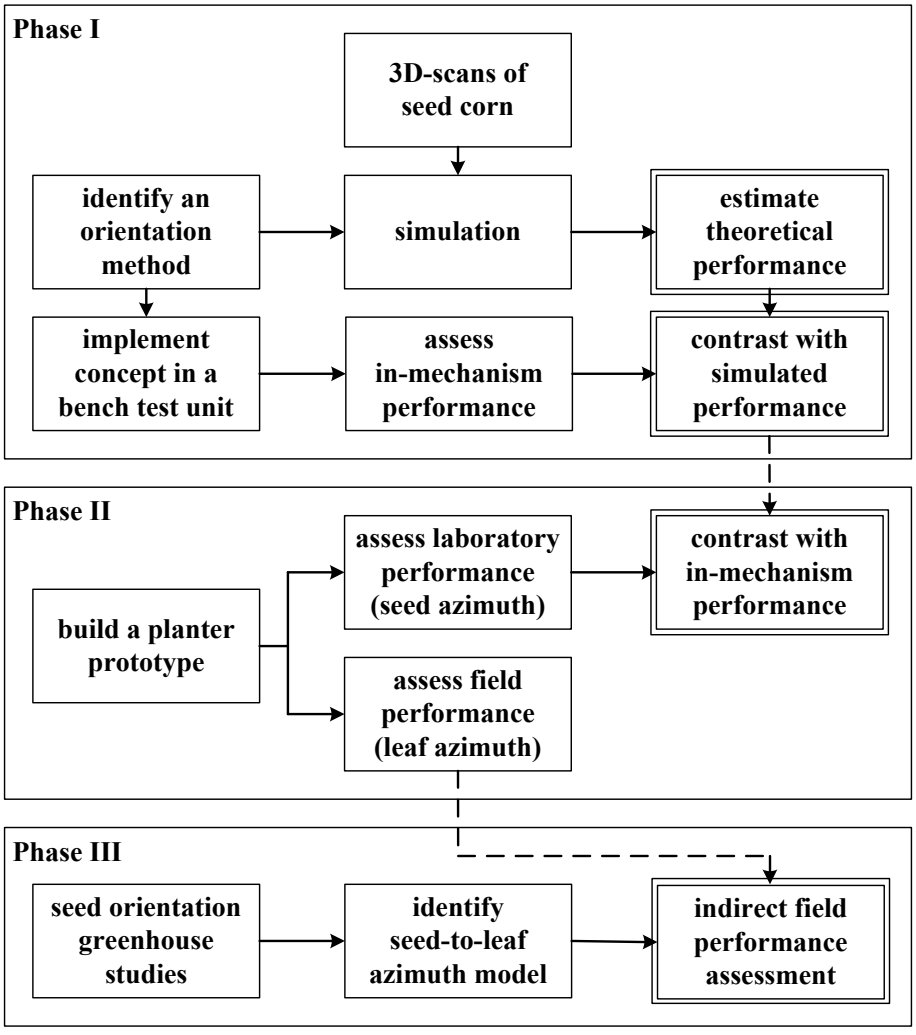

Figure 8. Overview of the three phases of the research plan.

In Phase I, the concept of seed orientation by unidirectional pushing is introduced. Orientation calculations with 3D data of corn seed laser scans are presented. Then, the realization of the concept in a bench unit is discussed and the in-mechanism performance results presented and contrasted with the predicted performance. In Phase II the prototype design is introduced and the results from laboratory tests compared with the conclusions from Phase I and II. The leaf azimuth data recorded in the field is also discussed. Phase III represents a feasibility assessment of a post-emergence seed orientation performance measure that allows the indirect determination of orientation accuracy in the field.

Common Materials and Methods

Some of the materials and methods used and/or applied throughout this work are common to all three phases. They are introduced in the following. The phase-specific materials and methods are introduced at their respective place in the document.

Test Seeds

Seeds of four corn hybrids – Monsanto DKC-6342 and DKC-6346 and Pioneer P0902HR and P1162HR, were used throughout the subsequent experiments. These hybrids were selected because the shapes of their kernels differ quite significantly from hybrid to hybrid. Figure 9 depicts typical kernels of the four hybrids. The kernels of DKC-6342 were quite cuboid with nearly parallel sides and a flatter area opposite the caryopsis attachment point. The kernels of DKC-6346 had more converging sides but still the same flat area opposite the tip. The kernels of the P0902HR resemble the shape of DKC-6346 but do not possess the flat area opposite the tip. The kernels of P1162HR on the other hand are quite discoidal. The grading for all hybrids was “medium flat”. In the context of this research, the terms “hybrids”, “kernels”, “seeds” are used interchangeably and refer to the seed kernels of the four test hybrids with the grading “medium flat”.

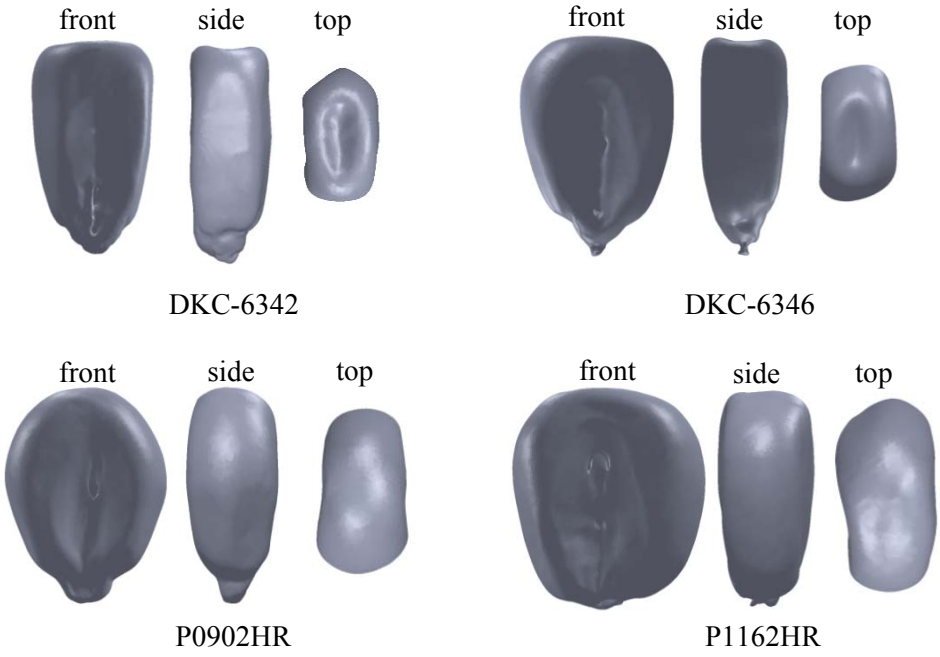

Figure 9. Front, side and top views of typical kernels of the four test hybrids. These four hybrids were selected because their typical "medium flat" kernels differ in shape quite significantly.

Tools of Circular Statistics

Data in angular or directional form is quite widely encountered in various sciences. Our three-dimensional environment makes it frequently a natural choice to record data in terms of directions or angles. Often, three-dimensionality can be reduced to two by a simple rotation of the reference system such that the majority of the effect of interest is captured in a plane. Although such data is abundant, sound statistical methods for handling directional measurements started only developing the late 1960s (Fisher, 1996).

As described by Mardia and Jupp (2000) "the sample space is typically a circle… so that standard methods for analyzing univariate or multivariate measurement data cannot be used. Special directional methods are required which take into account the structure of these sample spaces". The main issue with the application of methods intended for linear infinite spaces to circular data

lies in the fact that on the line, 0° and 359° are 359° apart. On the circle these two measurements could equally be only 1° apart. The higher the concentration of the measurements the smaller the error between the two classes of methods. After all, the "0°-direction" in highly concentrated data can always be chosen such that "the circle can be cut open at the most convenient location" (Fisher, 1996). In such cases, the mean, for example, from the linear domain closely agrees with the directional mean.

The methods applied in the context of this research follow the elaborations in the three major references for circular statistics. Batschelet (1981), Fisher (1996), and Mardia and Jupp (2000) have compiled exquisitely detailed guidelines for dealing with circular data. The key concepts are introduced in the following and then used throughout the remainder of this work without further explanation.

Circular Mean, Variance, and Standard Deviation

Each directional measurement can be regarded as a point on the unit circle. Therefore, the *mean direction* is defined as the direction of the resultant vector composed of the addition of all the unit vectors (Figure 10).

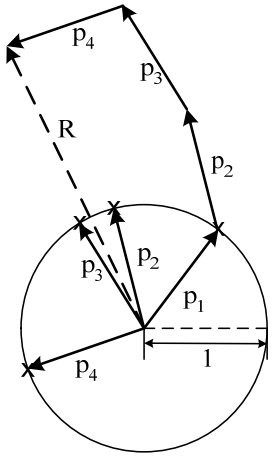

Figure 10. The resultant vector from the addition of all measurement points plotted on the unit circle has the direction of the mean direction. Figure adapted from Fisher (1996).

The mean resultant length, R_m, is then defined as

$$R_m = \frac{R}{n} \tag{1.1}$$

where n is the number of measurements. R_m is bounded between 0 and 1 and is at the same time a measure for the concentration of the data. The closer R_m to 1 the more concentrated the data. Therefore, the *sample circular variance* V_s defined as

$$V_s = 1 - R_m \tag{1.2}$$

is a measure for the lack of concentration in the data.

The *circular standard deviation* on the other hand is not as one might expect simply the square root of V. Its particular definition depends on the underlying probability distribution. The definition for the particular case of the von Mises distribution is introduced below.

Assessment of Uniformity

A formal test for uniformity is the *Modified Kuiper V test*. The hypothesis that the sample was drawn from a uniformly distributed population is rejected if the test statistic exceeds a critical value. The advantage of this test is that it makes no assumption about the alternative. The test simply assesses whether or not the underlying distribution of the sample could be uniform or not. Multi-modal models, which can be very difficult to distinguish from uniform distributions, can be detected as possibly non-uniform. The test, described in Fisher (1996, p. 67), essentially computes a weighted sum of differences between the uniform quantiles and the sample quantiles. The critical values for V can be found in Table A5 in Fisher (1996, p. 225).

The von Mises Distribution

The wrapped normal distribution and the von Mises distribution are very similar symmetric, unimodal probability models governed by two parameters. In fact, a data-based distinction

between the two may be difficult and "sample sizes in the order of a few hundred might be needed…" (Fisher, 1996, p. 55). However, "the many optimal and desirable properties of the Normal distribution on the line are, for circular distributions, divided between the Wrapped Normal and the von Mises distribution". Because parameter identification for von Mises distributions is generally more convenient, it is prominently used where these two models would be appropriate. Since it is usually the model of choice, substantial computational libraries exist that provide the bulk of the tools that may be needed to work with von Mises distributions. The package used throughout this work is "CircStat" by Berens and Velasco (2009), an extensive and meticulously documented freely available MATLAB toolbox. Their implementations are based on the same three key references on circular statistics mentioned above.

The *probability density function* of the von Mises distribution associated with an angular random variable θ is defined as

$$f_{\mu,\kappa}(\theta) = [2\pi I_0(\kappa)]^{-1}\exp[\kappa\cos(\theta-\mu)] \tag{1.3}$$

for $0 \leq \theta < 2\pi$ and $0 \leq \kappa < \infty$.

The function I_0 is the modified Bessel function of the first kind of order zero (Mardia and Jupp, 2000, p. 50) and μ and κ are the mean direction and the concentration parameter, respectively. The *cumulative distribution function* of the von Mises model is then given by

$$F_{\mu,\kappa}(\theta) = [2\pi I_0(\kappa)]^{-1}\int_0^{\theta}\exp[\kappa\cos(\phi-\mu)]d\phi \tag{1.4}$$

of which, however, no close-form solution exists. Algorithms for numerical approximations can be found in Fisher (1996) and Batschelet (1981).

Estimates of the parameters μ and κ of a von Mises distribution are quite easily obtained. The circular mean of the data is already the maximum likelihood estimate of μ. The maximum

likelihood estimate of the concentration parameter κ can then be written in dependence of the mean resultant length R_m (Fisher, 1996, p. 88). However, the accuracy of the estimate is sensitive with respect to sample size (especially for n < 15) and the estimated value of κ. Estimating κ may therefore be an iterative process that requires switching methods depending on the initial estimates of κ.

The *circular standard deviation* For the von Mises model used throughout this work is defined by

$$\sigma_{vM} = \frac{1}{\sqrt{nR_m\kappa}} \tag{1.5}$$

Intervals for a 100(1-α)% confidence for the mean directions can therefore be computed by

$$\mu \pm sin^{-1}(z_{0.5\alpha}\sigma_{vM}) \tag{1.6}$$

where $z_{0.5\alpha}$ corresponds to the 100(1-0.5α)% point of the linear normal distribution.

The goodness of fit for a von Mises model can be assessed by the *Watson* U^2 test. For each sample point θ_i the cumulative frequency value z_i is computed using the estimated parameters κ* and μ*.

$$z_i = F_{\kappa*}(\theta_i - \mu^*), \qquad i = 1, \dots, n \tag{1.7}$$

These values are then arranged in ascending order

$$z_1 \leq \cdots \leq z_n \tag{1.8}$$

and with z_m given by

$$z_m = \sum_{i=1}^{n} \frac{z_i}{n} \tag{1.9}$$

the test statistic U^2 can then be obtained by

$$U^2 = \sum_{i=1}^{n} \left[z_i - \frac{2i-1}{2n} \right]^2 - n\left(z_m - \frac{1}{2} \right)^2 + \frac{1}{12n} \tag{1.10}$$

If U^2 exceeds a certain critical value, which depends on the desired significance level, the concentration parameter κ and whether or not μ and/or κ were a priori known (see Table A8 in Fisher, 1996, p. 230), the hypothesis that the sample was drawn from a von Mises distribution with estimated mean μ^* and concentration parameter κ^* is rejected.

A *mixture of two von Mises distributions* can be described by five parameters, as long as each contributing distribution is unimodal. The mean directions of the two modes are denoted μ_1 and μ_2 and the associated concentration parameters are κ_1 and κ_2, respectively. The fifth parameter p indicates the mixing ratio. To estimate these five parameters, the iterative least-square minimization algorithm described in Jones (2006) should be followed. Although Fisher (1996, p. 97) introduces the same procedure, typos in the algorithm outline may confuse the reader and lead to an incorrect implementation. Whether or not the least-square estimation algorithm actually converges depends on the data structure and the initial estimate. Fitting of mixture parameters may be unsuccessful despite prior testing indicated that the hypothesis of uniform distribution should be rejected.

Once von Mises parameters have been estimated it may be interesting to check if there is evidence that two or more models are statistically different. The concentration parameters and the mean directions are compared separately. Since the details of the comparison test for the mean direction depends on the outcome of the test for equality in the concentration parameters, it is common first to check whether not the concentration parameters can be assumed to be equal. The procedure can be found in Fisher (1996), p. 131. The critical value is taken from the F distribution. For example, comparing the estimates of κ_1 and κ_2 of two samples with n_1 and n_2 number of data points, respectively, the critical value for $\alpha = 0.05$ would be $F_{1,(n1+n2-2)}(P=0.95)$. If the test statistic exceeds the critical value, the hypothesis that κ_1 and κ_2 are equal must be rejected.

The method to compare the estimated means is known as the Y-test, described in Fisher, 1996, p.117 and p.124. The critical value is taken from the $\chi 2$ distribution. If the test for equality of the concentration parameter showed no significant difference, then an alternative version of the test may be used (Fisher, 1996, p.126).

References

Andrieu, B., N. Ivanov, and P. Boissard. 1995. Simulation of light interception from a maize canopy model constructed by stereo plotting. *Agricultural and Forest meteorology* 75(1-3):103-119.

Batschelet, E. 1981. Circular statistics in biology. *Academic Press, New York.*

Berens, P., and M. J. Velasco. 2009. CircStat: A MATLAB Toolbox for Circular Statistics. *Journal of Statistical Software* 31(10).

Blad, B. L. B., and D. G. Baker. 1972. Orientation and Distribution of Leaves Within Soybean Canopies. *Agronomy Journal* 64(1):26.

Chelle, M., J. Hanan, and H. Autret. 2004. Lighting virtual crops: the CARIBU solution for open L-systems. Citeseer.

Code of Federal Regulations. 2012a. Title 7, Part 201 – Federal seed act regulations. Available at: http://ecfr.gpoaccess.gov. Accessed March 15, 2012.

Code of Federal Regulations. 2012b. Title 7, Part 810 – Official United States standards for grain. . Available at: http://ecfr.gpoaccess.gov. Accessed March 15, 2012.

Fisher, N. I. 1996. *Statistical Analysis of Circular Data*. Cambridge University Press.

Fortin, M. C., and F. J. Pierce. 1996. Leaf azimuth in strip-intercropped corn. *Agronomy Journal* 88(1):6-9.

Jones, T. A. 2006. MATLAB functions to analyze directional (azimuthal) data - I: Single-sample inference. *Computers & Geosciences* 32:166 - 175.

Liu, W. D., M. Tollenaar, G. Stewart, and W. Deen. 2004. Impact of planter type, planting speed, and tillage on stand uniformity and yield of corn. *Agronomy Journal* 96(6):1668-1672.

Loomis, R., and W. Williams. 1969. Productivity and the morphology of crop stands: patterns with leaves. *Agronomy--Faculty Publications*:187.

Lopez-Lozano, R., F. Baret, M. Chelle, N. Rochdi, and M. Espana. 2007. Sensitivity of gap fraction to maize architectural characteristics based on 4D model simulations. *Agricultural and Forest meteorology* 143(3-4):217-229.

Maddonni, G., M. Chelle, J. L. Drouet, and B. Andrieu. 2001. Light interception of contrasting azimuth canopies under square and rectangular plant spatial distributions: simulations and crop measurements. *Field crops research* 70(1):1-13.

Maddonni, G., and M. Otegui. 1996. Leaf area, light interception, and crop development in maize. *Field crops research* 48(1):81-87.

Maddonni, G. A., M. E. Otegui, B. Andrieu, M. Chelle, and J. J. Casal. 2002. Maize leaves turn away from neighbors. *Plant Physiology* 130(3):1181.

Mardia, K. V., and P. E. Jupp. 2000. *Directional Statistics*. Wiley Series in Probability and Statistics. Wiley and Sons, Chichester, UK.

McComb, W. N. 1915. Seed Tape. United States Patent Office, 1'143'980.

Monsanto Imagine. 2008. Does Corn Seed Size and Shape Really Matter? *Agronomic Spotlight*.

OECD.2011.Schemes for the varietal certification or the control of seed moving in international trade. Paris.

Paliwal, R. L., G. Granados, H. R. Lafitte, and A. D. Vlollc. 2000. *Tropical Maize: Improvement and Production*. Food and Agricultural Organisation of the United Nations, Rome.

Peters, D., and J. T. Woolley. 1959. Orientation Planting Means More Moisture. *Agricultural Research* Vol. 7(No. 9):6-7.

Singer, J. W. C., W. J. Hahn, R. R. Shields, and J. Elson. 2000. Cropping system effects on weed emergence and densities in corn. *Agronomy Journal* 92(4):754.

Stewart, D., C. Costa, L. Dwyer, D. Smith, R. Hamilton, and B. Ma. 2003. Canopy structure, light interception, and photosynthesis in maize. *Agronomy Journal* 95(6):1465-1474.

Toler, J. E., E. C. Murdock, G. S. Stapleton, and S. U. Wallace. 1999. Corn leaf orientation effects on light interception, intraspecific competition, and grain yields. *Journal of Production Agriculture* 12(3):396-399.

Tollenaar, M., A. Dibo, A. Aguilera, S. Weise, and C. Swanton. 1994. Effect of crop density on weed interference in maize. *Agronomy Journal* 86(4):591-595.

Torres, G., J. Vossenkemper, W. Raun, and R. Taylor. 2011. Maize (Zea Mays) Leaf Angle and Emergence as Affected by Seed Orientation at Planting. *Experimental Agriculture* 1(1):1-14.

Torres, G. M. 2012. Precision Planting of Maize (Zea mays L.) (doctoral dissertation). Oklahoma State University, Department of Plant and Soil Science, Stillwater, OK.

USDA-FAS. 2012a. Corn Area, Yield, and Production. Available at: http://www.fas.usda.gov/psdonline/psdgetreport.aspx?hidReportRetrievalName=BVS&hidReportRetrievalID=884&hidReportRetrievalTemplateID=1. Accessed June 5, 2012.

USDA-FAS. 2012b. World Corn Production, Consumption, and Stocks. Available at: http://www.fas.usda.gov/psdonline/psdgetreport.aspx?hidReportRetrievalName=BVS&hidReportRetrievalID=459&hidReportRetrievalTemplateID=7. Accessed January 5, 2013.

Westgate, M., F. Forcella, D. Reicosky, and J. Somsen. 1997. Rapid canopy closure for maize production in the northern US corn belt: Radiation-use efficiency and grain yield* 1. *Field crops research* 49(2-3):249-258.

Williams, D. E. 1965. Groove forming, seed orienting planter shoe. United States Patent Office 3,217,674.

CHAPTER II

PHASE I: SEED ORIENTATION BY PUSHING

After a short overview of deployed techniques for part feeding in industry, this chapter introduces the concept of orientation by pushing. The concept is then applied to three-dimensional data obtained from laser scans of actual seed corn which leads to a first performance estimate of seed orientation by pushing.

Industrial Part Feeding

Part handling, sorting, orienting and positioning are very important tasks in a wide range of industries. In packaging for example, bottle caps are bulk fed to mechanical systems that orient and position them such that passing bottles may be sealed at astounding rates. Pills, vials, tubes, etc. for example in the pharmaceutical industry undergo similar processes to combine the product with its label and wrapper. It is therefore appropriate to review some of the state of the art technologies employed in these industries.

Vibratory Part Feeders

Many industrial part feeders use vibratory agitation or centrifugal forces to move and/or rotate parts into a specified position and orientation. The vibratory feeder depicted in Figure 11 singulates and orients plastic extrusion parts for the downstream process.

These vibratory or centrifugal force systems are customized to handle one specific part. The vibration frequency and amplitude or the rotational speed is adjusted to that particular component. Quite extensive fine-tuning is often necessary to achieve the desired performance (Mitchell, 2011). For proper functional performance, the designs of such vibratory feeders rely heavily on the fact that the parts are very uniform in shape and mass.

Figure 11. Many industrial part feeders use vibratory or centrifugal force agitation for part positioning and/or orientation. The depicted 21" bowl feeder by Service Engineering, Inc. advances 20 parts per minute to the next processing step.
Image by courtesy of Service Engineering, Inc.
http://www.serviceengineering.com/

Mitchell's discussion makes it apparent that the use of a vibratory feeder system for seed orientation may not be recommendable. The variability among the seeds and the vibratory disturbances of the planter traveling down the field – both adverse boundary conditions for a vibratory part feeder – will render solving seed orientation through this approach a daunting task.

Pick-and-Place Manipulators

The semiconductor industry deploys highly advanced pick-and-place machines to populate PCBs with electronics components. The latest machinery, as for example developed by JUKI (http://www.juki.co.jp/), may place and solder up to 90,000 parts per hour. Again, such

performance can only be achieved if the supplied parts are highly uniform and presented the manipulator in a deterministic position and orientation.

Robotic handling of individual parts in assembly automation becomes quite complex if the position and the orientation of the part is not fully known. Today's most advanced systems are equipped with highly capable cameras that allow real-time image processing to detect the object and compute a feasible pick-and-place trajectory (Kuehnle et al., 2009; Torralba et al., 2003). This makes exact prior knowledge about the position and the orientation obsolete. Furthermore, these systems are capable of handling a mixture of various parts in a random order and execute a specific command depending on the type of part and the position and orientation detected.

A pick-and-place solution for seed orientation mechanization can be excluded at this time, because an implementation would have to address solutions to these three main steps:

1) Grasping of the seed by an actuator. While not trivial, this may be solvable with today's technology.
2) Determination of the seed orientation by appropriate sensing. This would likely involve imaging, possibly stereo vision and extraction of the required information from these images.
3) If the current orientation can in fact be determined to an acceptable degree of accuracy, a rotational and translational trajectory must be computed to orient the seed and place it in the ground at the correct location.

The complexity and cost of such a solution prohibits the prosecution of such a concept.

Part Alignment by Fence-on-Conveyor

Much more commonly used and much less costly systems for assembly part feeding use fences on a conveyer. The parts in random orientations are transported on a moving belt and so

encounter various fences at defined angles and positions that force the parts to slide on the transportation surface and thereby rotate (Figure 12). The mechanics of part orientation by sliding has been quite extensively studied. In-depth investigations by Mason (1982), Brost (1985, 1988) and Peshkin and Sanderson (1986a, b, 1988) laid solid foundations for much related research.

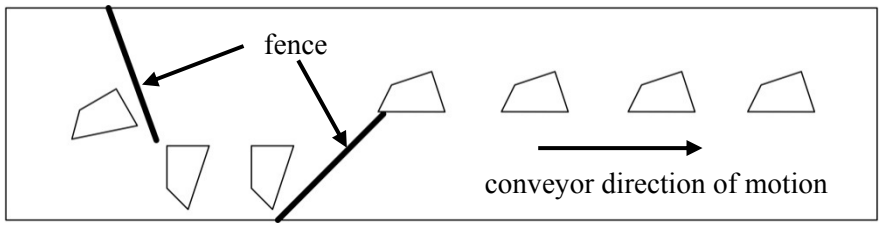

Figure 12. Part orientation by fence is commonly applied in assembly and packaging automation.

Alternatively, instead of passively forcing the parts around obstacles, the part may be actively pushed. The interaction between the pusher, the pushed object, and the support surface forces the part the rotate. This fundamental concept lies at the core of this research and is detailed in the following.

Part Orientation by Planar Pushing

The fundamental idea of planar pushing is depicted in Figure 13. A plane moves towards an object, makes contact at the closest point and forces the object to rotate and/or translate.

Assumptions

At this point, the key assumptions are introduced and justified. These are in close accordance with those put forth by Brost (1985) and later Goldberg (1993).

1) Any three-dimensional object can be approximated as a polyhedron. An arbitrary spatial resolution may be achieved by selecting the desired number of vertices.

   → For objects with a piece-wise continuous surface, the Weierstrass theorem assures that the surface can be approximated arbitrarily close by a set of polynomial functions.

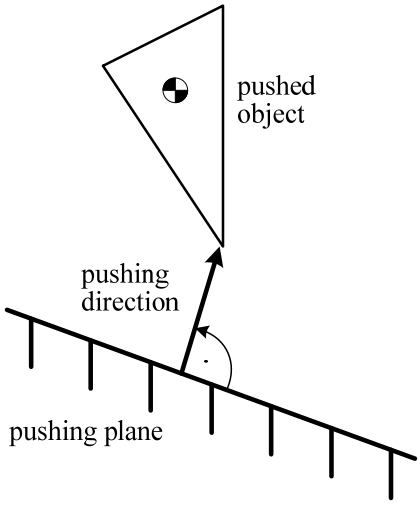

Figure 13. Planar pushing: A plane moves towards an object, makes contact at the closest point and starts pushing the object, forcing it to rotate and translate.

2) All motion occurs in a plane.

   → Any polyhedral, sufficiently oblate object will topple when pushed until a stable, or natural, resting aspect is attained. A detailed treatment on this subject can be found in Lee et al. (1996) and Lynch (1999a, b).

   → It follows from 1) and 2) that any polyhedral object resting in a stable position on a plane can then be approximated by a polygon by projection onto the support plane.

3) For the purpose of this analysis, the pushing plane is considered to extend to infinity.

   → It follows from 1), 2) and 3) that any polyhedral object may be approximated by a *convex* polygon in the support plane because the pushing plane will not be able to make contact at any point not on the convex hull of the polygon.

4) The direction of pushing is orthogonal to the pushing plane.

   → By design of the orientation concept, one may choose to enforce this assumption.

5) The center of mass of the pushed object is coincident with the volumetric centroid of the polyhedron.

   → If the density of the object is uniform throughout the volume, this assumption holds

directly from the definition of the location of the centroid. For this study, it is assumed that the mass properties of the corn seeds are uniform throughout the seed. Since a corn seed is composed of several distinct elements, as described, for example, by Singh et al. (1991) this may not be entirely accurate. However, determination of density variations throughout corn seeds lies outside the scope of this study.

6) The center of friction of the object on the support plane is coincident with the centroid of the projection polygon.

   → Realistically, the irregularly curved surface of a corn seed will make contact with the support surface at three points, forming a locally stable tripod support. The true center of friction lies at the centroid of the pressure distribution among the three points (Mason, 1982). However, as the seed is pushed, the tripod support may transition rapidly from one configuration to another and average out over the set of all possible tripod configurations (Peshkin and Sanderson, 1986b).

Radius and Push Function

For conditions under which the above assumptions hold, Goldberg (1993) showed that the behavior of pushed parts can be described by two functions. The *radius function* is defined by the distance between any point on the perimeter of the polygon and the centroid of the pushed object. The calculated distances are ordered along the perimeter of the polygon, resulting in a function with a period of 2π. Goldberg (1993) went on to show that, when pushed, the part will rotate such that eventually the pushing contact coincides with the closest local minimum. Figure 14 depicts a sample polygon with four vertices. The tetragon's coordinates system is indicated in the figure and located at the centroid. The measure of positive angles is also marked. Starting at an angle of 0°, the distance of any point on the perimeter to the centroid can be computed. The result is the radius function depicted in Figure 15a). The approach direction of the pushing plane is now

rotated around the tetragon. As the plane approaches the tetragon, the closest vertex will always contact the plane first.

At certain critical angles, when the approach direction passes the line formed by the centroid and the closest vertex, the direction of rotation of the tetragon changes sign. The radius function illustrates that: the positive peaks in Figure 15a) correspond to the angles of the vertices measured in the coordinate system of the tetragon. These transition points located on the perimeter of the polygon are defined as *reversal point*.

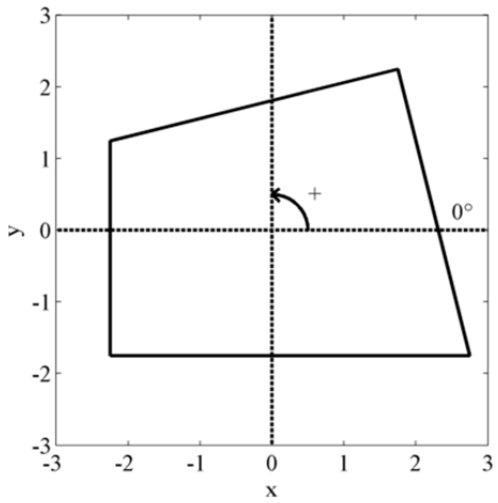

Figure 14. An example polygon with 4 vertices is used to illustrate the concepts of the radius and push functions.

Between the peaks, the tetragon will rotate to the angle indicated by the local minimum of the radius function. The corresponding points on the perimeter of the polygon are referred to as *stable points*. The *push function* therefore becomes the piece-wise constant function depicted in Figure 15b). Any approach angle between the transition points rotates the tetragon to the locally stable aspect dictated by the radius function.

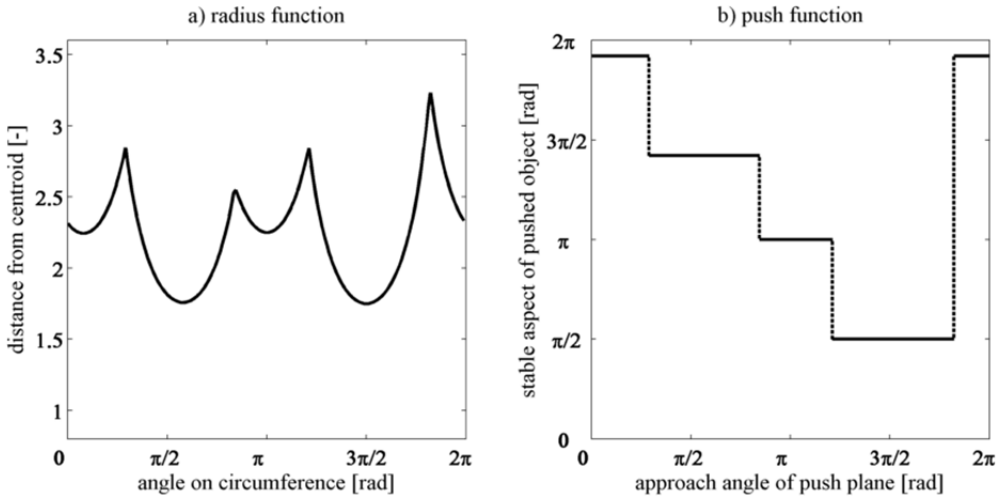

Figure 15. The computed radius and push functions for the tetragon in Figure 14.

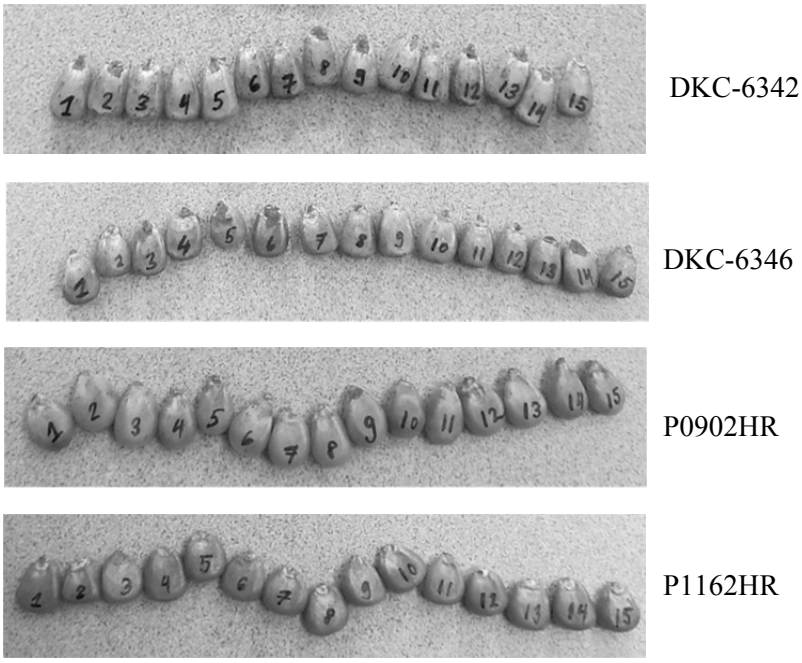

Figure 16. Fifteen seeds of each hybrid were randomly selected, numbered, and sent for 3D laser scanning.

Simulation of Seed Orientation by Pushing

Of each of the four hybrids introduced above, 15 seeds were randomly selected, numbered and sent for 3D laser scanning (see Figure 16). The service was provided by arrival3D, Inc. , Coweta,

OK (http://www.arrival3d.com/). Laser scanning produced point clouds containing anywhere from roughly 120,000 to 1,100,000 points. Handling of the data was facilitated by triangular meshing of the point clouds into polyhedrons which reduced the number of data points significantly to about 6,000 vertices per seed scan. The meshed polyhedron served as the input to the calculations described below.

Seed Reference Systems

At this point, it is necessary to introduce a coordinate system that is fixed with respect to the seed. As depicted in Figure 17, this reference system is attached at the seed's center of mass. By Assumptions 5) and 6) from above, the center of mass is considered coincident with the volumetric centroid. The x-axis of the seed, x_s, points from the centroid to the caryopsis attachment point. The z-axis, z_s, is perpendicular to the "mid plane" of the seed and points in the direction where the embryo is located. The y-axis, y_s, lies in the "mid plane" of the seed and completes the right-handed coordinate frame. A more precise mathematical definition of the axes directions will become apparent when the reference system is regarded in combination with the three-dimensional data.

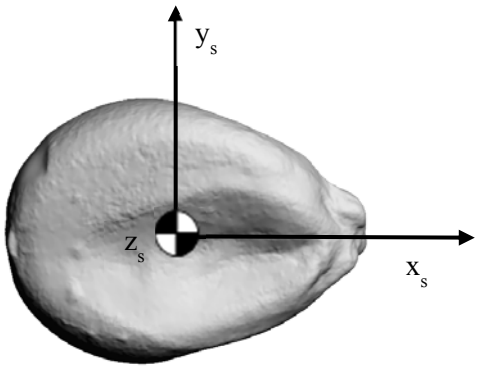

Figure 17. The coordinate system of the seed is attached at the center of mass. Its x-axis points along the largest dimension of the seed towards the caryopsis attachment point.

Computational Details

A schematic of the sequence of the computational pushing calculations is shown in Figure 18. Some of the key operations listed are discussed below. The algorithm was implemented in MATLAB (The MathWorks Inc., 2011).

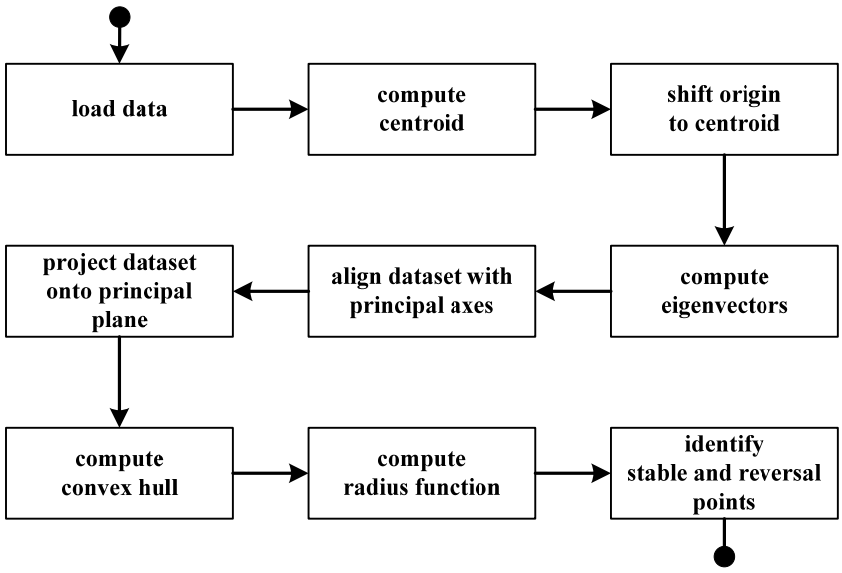

Figure 18. The sequence of the computational pushing analysis.

Translation of the Data to the Centroid:

The computation of the centroid of a point cloud is not trivial. The straight-forward method of simply averaging the coordinates of all vertices assumes that the points are uniformly distributed through space. This is clearly not correct in this case. While the point density of the original laser scanner output was relatively uniform, the sheer number of data points makes such files difficult to handle. The triangulation into a mesh reduced the number of vertices greatly, however, with the result that areas of higher curvature have a much higher vertex density.

For this study, a method described by O'Rourke (1998) was followed. The polyhedron is decomposed into Euclidian simplices of which the individual centroids are easily computed. The polyhedron's location of the centroid then is a weighted average of the locations of the centroids

of these simplices with the weights being the volumes thereof. The triangulation of the point cloud of a scanned seed produced a polyhedron with a surface exclusively composed of triangles. The simplices were therefore constructed with the triangles as bases and the origin of the original data set as the forth common vertex for all simplices. The volume of the i-th simplex with one vertex located at the origin and the locations of the three remaining vertices denoted by vectors $\mathbf{x_i}$, $\mathbf{y_i}$, and $\mathbf{z_i}$ is given by

$$V_i = \frac{\langle \boldsymbol{x_i},\ \boldsymbol{y_i} \times \boldsymbol{z_i} \rangle}{6} \tag{2.1}$$

The location of the centroid, $\mathbf{c_i}$, of each simplex can be computed by

$$\boldsymbol{c_i} = \frac{1}{4}(\boldsymbol{x_i} + \boldsymbol{y_i} + \boldsymbol{z_i}) \tag{2.2}$$

thereby providing all the necessary input for the determination of the centroid, $\mathbf{c_s}$, of the polyhedron using

$$\boldsymbol{c_s} = \frac{\sum_{i=1}^{n} V_i\, \boldsymbol{c_i}}{\sum_{i=1}^{n} V_i} \tag{2.3}$$

The origin of the data was subsequently translated to coincide with this centroid.

Alignment with Principal Axes and Projection onto Support Plane:

To determine the direction of the coordinate axes, a principal component analysis on the set of vertices was performed. The eigenvectors of the covariance matrix produce the orthonormal basis which was chosen as the axes of the coordinate system. Coincidently, the eigenvector associated with the largest eigenvalue can be chosen as the direction of x_s because it always points along the long axis of the seed towards the caryopsis attachment point. The eigenvector associated with the second largest eigenvalue can be denoted y_s and the remaining direction is z_s. While this observation may not be true for all seed grades, it holds for “medium flats” and is very convenient for the subsequent calculations.

The support plane was then defined as the plane formed by the axis x_s and y_s. The projection $\mathbf{v_{ip}}$ of each vertex $\mathbf{v_i}$ onto the support plane is obtained simply by

$$\boldsymbol{v_{ip}} = \begin{bmatrix} v_{ix} \\ v_{iy} \\ 0 \end{bmatrix} \tag{2.4}$$

Computation of the Stable and Reversal Points:

As shown in Figure 19, the computation of the convex hull of the projection of all vertices onto the support plane yields the polygon relevant for the pushing calculations. The radius function of that polygon is shown in Figure 20a). The extrema of the radius function can be determined by examination of the zero crossings of the first derivative. Inspection of the second derivative allows the distinction between minima and maxima. It is immediately apparent that the degree of stability of the three stable points differs significantly. The stable point at the approximate angular location of π is a far weaker minimum than the two alternative minima at roughly π/2 and 3π/2. Ideally, the stable points would be located *exactly* at π/2 and 3π/2 because this would align the x-axis of the seed with push plane which is the primary objective.

The push function for this particular seed depicted in Figure 20b) shows that the push plane approach angle for stability around π is quite small (roughly 60° or π/3). Any other approach angle will result in a final orientation at one of the other two stable points.

The angular values of stable and reversal points can be translated to points on the perimeter of the polygon by interpolating for the closest value in the vector of vertices (Figure 21). Also indicated in the figure are the three possible final stable aspects of the push plane.

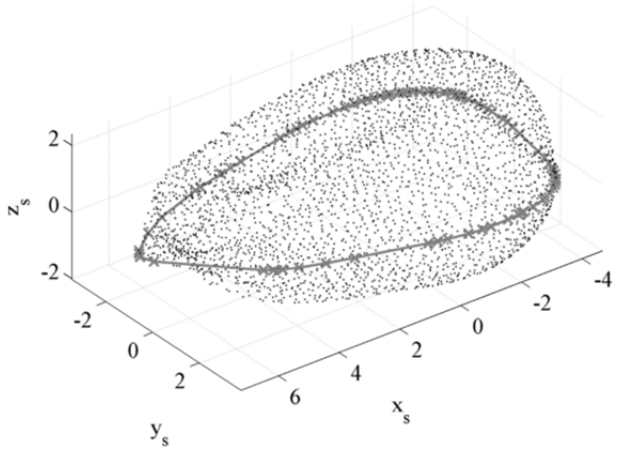

Figure 19. The convex hull of the projection of the vertices onto the support plane spanned by x_s and y_s yields the polygon relevant for the pushing calculations (Seed 15, DKC-6342).

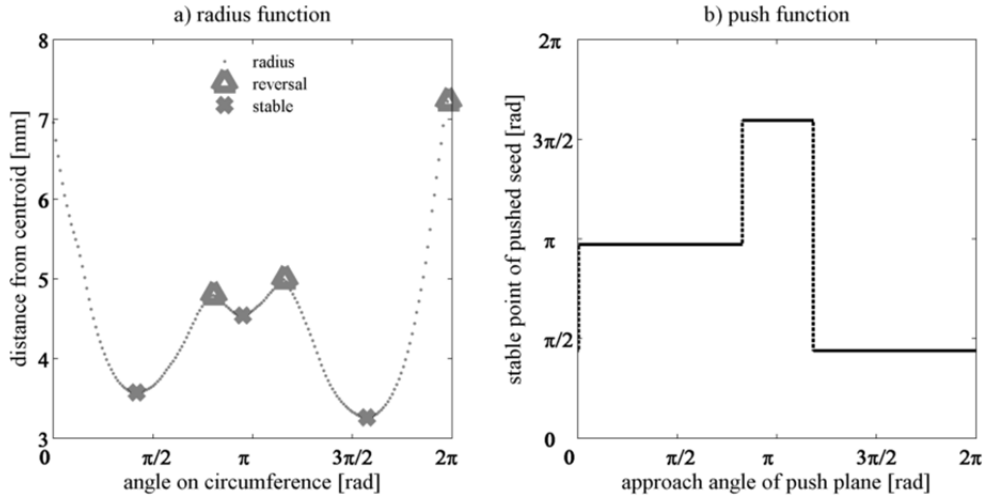

Figure 20. The extrema of the radius functions determine the stable and reversal points (Seed 15 of DKC-6342).

The location of the reversal points may now be used to calculate a probability for each stable point. Assuming a seed's initial orientation is uniformly random then the probability of the final orientation at a certain stable point is proportional to the angle between the reversal points that lie clockwise and counterclockwise from the stable point. For example in Figure 21, if the initial contact point of the pushing plane lies between RP_1 and RP_2 then the pushing plane will

eventually make contact with the seed at SP_1. Similarly, if the initial contact point is between RP_2 and RP_3 or between RP_3 and RP_1, the seed orientation will be determined by the stable points SP_2 and SP_3, respectively. For the particular seed depicted in Figure 21, the probabilities associated with SP_1, SP_2, and SP_3 are 0.41, 0.42, and 0.17, correspondingly.

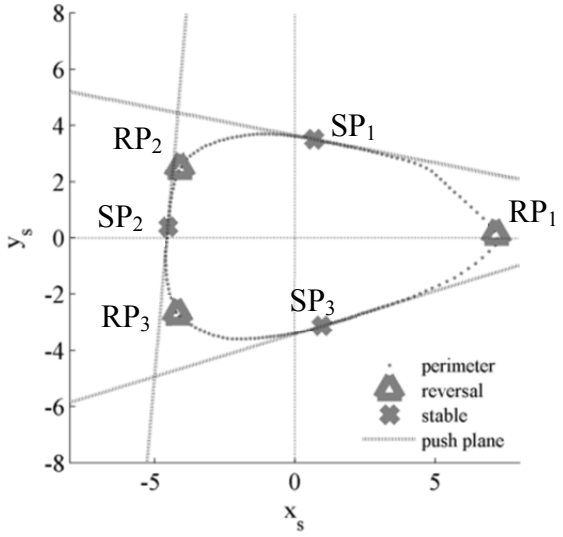

Figure 21. The stable and reversal points on the perimeter of Seed 15 of DKC-6342.

Results of Simulated Orientation Performance

The 15 seeds of each of the four hybrids were processed and the stable and reversal points computed. While the hybrids DKC-6342 and DKC-6346 consistently show three stable points, it is noteworthy that the hybrid P0902HR exhibits only two stable points around the circumference. The radius function of P0902HR does not possess a local minimum near π while the hybrids DKC-6342 and DKC-6346 consistently show three points. The kernels of the hybrid P1162HR are still sufficiently oblate and elongated that the above calculations produce a meaningful definition of the reference coordinate system and hence angle measurements. However, because of its nearly discoidal shape often several, weakly stable points are found around the circumference. The radius function of Seed 5 of P1162HR is depicted in Figure 22. It can be seen

that for this particular seed at least 5 local minima can be identified. For comparison with the other hybrids, the three strongest local extrema were considered relevant.

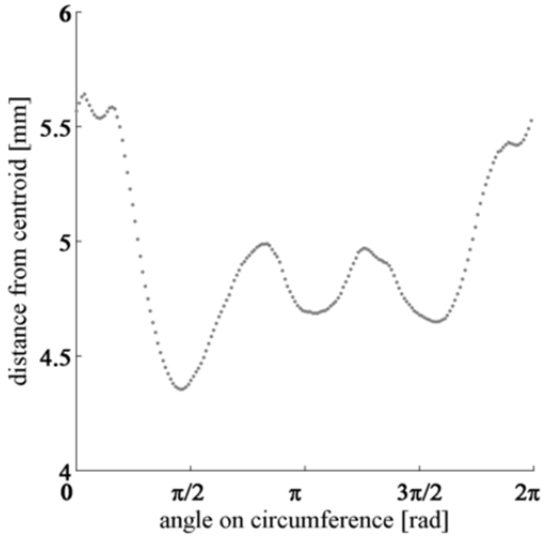

Figure 22. The radius function for Seed 5 of P1162HR.

For the hybrid DKC-6342 the circular histograms for the stable points and the reversal points for all 15 seeds are depicted in Figure 23. The radial direction indicates fractions or probabilities associated with a particular direction. As evident from the graph, the angular variability of the stable and reversal points across the seeds within the medium flat kernels of this specific hybrid is small. Note that the stable and reversal points are shown in the reference frame of the seed. The 0°-direction indicated in the histograms refers to the direction of x_s.

As evident from Figure 24 the kernels of DKC-6346 exhibit very similar characteristics as DKC-6342. The stable and reversal points are grouped at three angular orientations. In comparison with DKC-6342, the variability of the angular location of the stable points is somewhat greater. The circular histogram of P0902HR depicted in Figure 25 confirms that only two stable points around the circumference can be identified. The reversal points opposite the caryopsis attachment point are more scattered than for kernels of the hybrids. The stable and reversal points of the kernels of P1162HR are more variable as evident from Figure 26.

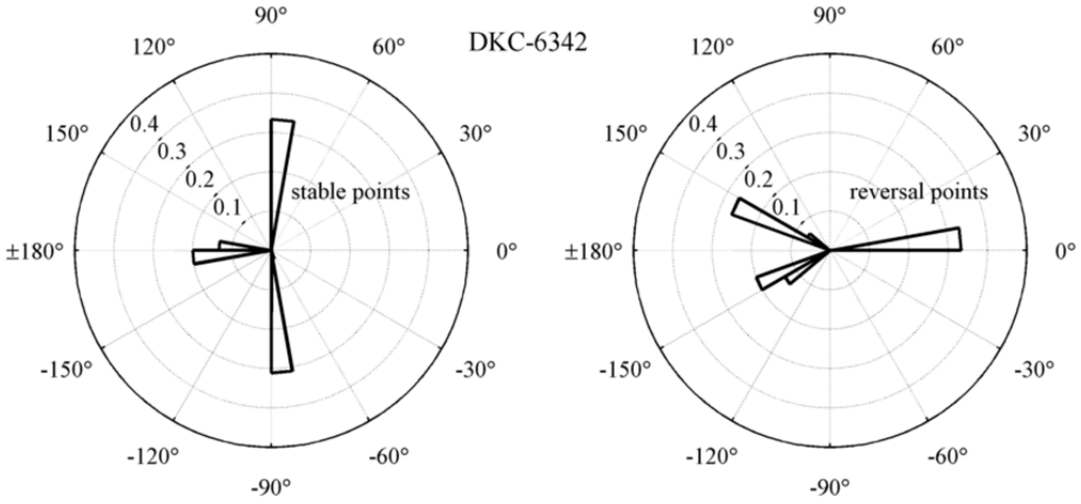

Figure 23. The stable and reversal points on the perimeter of 15 medium flat kernels of DKC-6342.

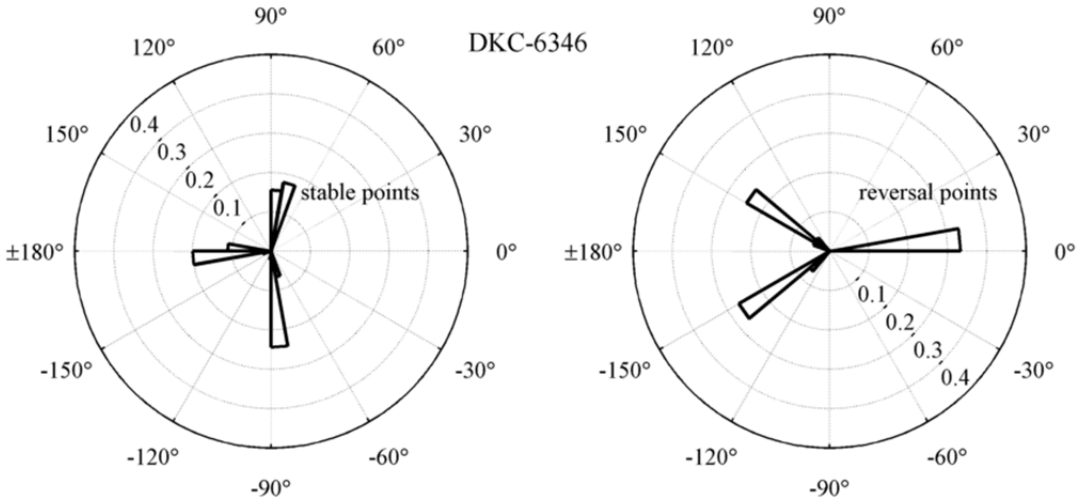

Figure 24. The stable and reversal points on the perimeter of 15 medium flat kernels of DKC-6346.

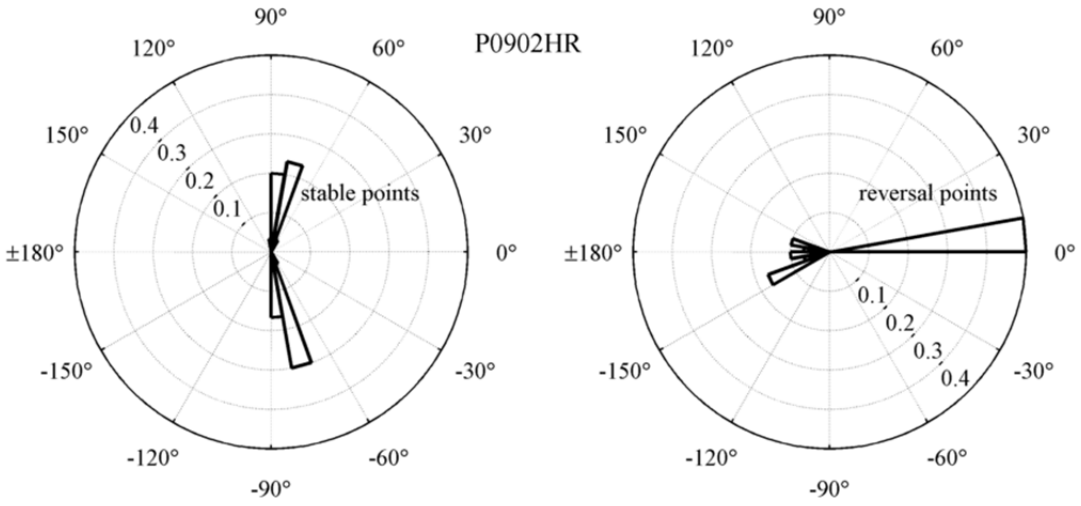

Figure 25. The stable and reversal points on the perimeter of 15 medium flat kernels of P0902HR.

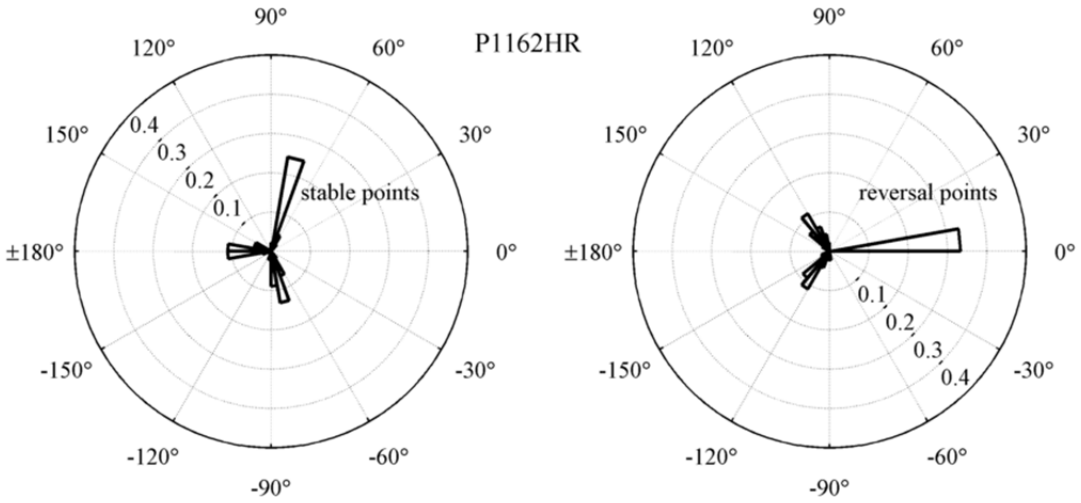

Figure 26. The stable and reversal points on the perimeter of 15 medium flat kernels of P1162HR.

The summary of the stable point analysis of all hybrids is collected in Table 1. The listed mean direction μ and standard deviation σ (in brackets) are the circular types as introduced above. For better readability, the angles in Table 1 have been converted to degrees and constrained to ±180°. Note, while the stable and reversal points are generally sequentially numbered in

counterclockwise direction around the circumference, SP_2 for P0902HR is skipped for better comparison with the other hybrids. The probability associated with each stable point is also indicated. The indicated probabilities are the mean of the probabilities of the individual seeds.

Hybrid	SP_1[μ (σ)°]	$P(SP_1)$	SP_2[μ (σ)°]	$P(SP_2)$	SP_3[μ (σ)°]	$P(SP_3)$
DKC-6342	84 (3.2)	0.42	-179(3.4)	0.15	-83 (2.4)	0.43
DKC-6346	80 (3.6)	0.40	-178 (4.1)	0.20	-83 (5.3)	0.40
P0902HR	81 (7.2)	0.50	n/a	n/a	-77 (5.9)	0.50
P1162HR	74 (6.1)	0.34	176 (10.7)	0.31	-76 (11.4)	0.35

Table 1. Summary of the stable point analysis.

As evident from Table 1, both DKC hybrids appear to be very consistent. The calculated stable orientations at around ±80 degrees are close to the desired orientation of ±90 degrees for across-row orientation. The circular standard deviation of the stable points is only in the order of a few degrees. The main difference between hybrids that possess a flat end opposite the tip (DKC hybrids) and P0902HR, which is fairly rounded, is missing stable point at around $\pm\pi$ for P0902HR. The variability among the stable points for P0902HR is greater than for the kernels of the DKC hybrids. The data shows that the kernels of P1162HR are not very suitable for seed orientation by pushing because the two stable points of interest near ±90° are on average roughly 15° off from the desired orientation of ±90 degrees and the variability is higher than for kernels of the other hybrids.

The results of the reversal point analysis can be found in Table 2. The caryopsis attachment point at 0° is a reversal point for all hybrids. The small standard deviation associated with RP_1 as indicated in the table is attributable to the fact that a discrete number of points exist around the circumference. Therefore, the numerical analysis may at times identify a point to the left or the right of 0° as the local maximum. As already seen in the stable point analysis both DKC hybrids exhibit fairly similar properties. The only other reversal point for P0902HR besides RP_1 at 0° lies nearly opposite at roughly -173°. The reversal points of the kernels of P1162HR are nearly

equally spaced around the circumference at intervals of 120 degrees. Hence, the probability of ending up at any of the three stable points is roughly 0.33.

Hybrid	RP_1[μ (σ)°]	RP_2[μ (σ)°]	RP_3[μ (σ)°]
DKC-6342	0 (0.5)	152 (3.5)	-150 (3.4)
DKC-6346	0 (0.4)	145 (4.4)	-144 (4.6)
P0902HR	0 (0.4)	n/a	-173 (12.9)
P1162HR	0 (0.5)	121 (13.0)	-125 (15.9)

Table 2. Summary of the reversal point analysis.

The variability of the reversal points of the DKC hybrids is the same order as the variability of the stable point indicated in Table 1. The variability among the reversal points for the kernels of the hybrids P0902HR and P1162HR is much higher as indicated by the larger standard deviations.

Model Validation in Bench Tests

Mechanization of seed orientation may be approached in two fundamentally different ways: Either the seeds are first oriented and then placed at the correct spacing in the ground while maintaining the orientation or the seed is placed (or dropped) into the furrow and then oriented as it already sits on the ground. In both cases, it might be possible to apply the concept of orientation by pushing. In the context of this work, exclusively the first approach was investigated.

Mechanism Concept Based on Profiled Belt

On modern planters, seeds are typically metered and then dropped 40 to 50 cm through a tube into the furrow. Once the seed is oriented, it can no longer be dropped to the ground since the orientation would likely be lost in the transition. The release point of the seed had to be set as close to the ground as possible. Continuous operation was considered a key requirement. Therefore, implementing a profiled belt at the core of the design, as depicted in Figure 27, comes with several advantages. The belt can be kept narrow to allow the mechanism to be placed in the seed furrow very close to the ground. As the seed enters the mechanism at an arbitrary orientation, it is caught by the profile on the belt and pushed along. The seed is thereby oriented

before it is released to the ground. As schematically shown in Figure 28, the release point of the seed is at the bottom of the seed furrow only the thickness of the bottom plate above ground (roughly 3.5 mm).

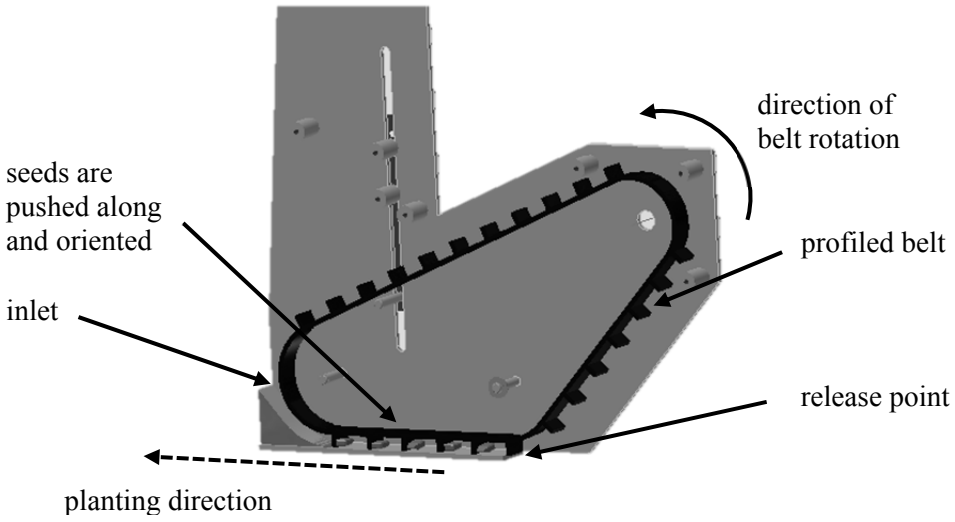

Figure 27. The profiled belt is at the core of the orientation concept. The seeds enter the mechanism, are caught be the teeth and pushed along and thereby oriented before release to the ground.

As the seeds get caught by the belt and are pushed along, they must be free to rotate and align themselves with the pushing plane. Therefore, the cavities on the profiled belt must provide enough room for the seeds to slide and rotate. Because the seed release point must be located at the very bottom of the seed furrow, the belt should be kept as narrow as possible to minimize the width of the furrow. Jayan and Kumar (2004), Coskun et al. (2006), Isik and Izli (2007) have published detailed data on the physical properties of corn seeds, including dimensional data of kernel shapes. Based on their measurements, an average seed is roughly 10 mm long, 8 mm wide, and 4 mm thick.

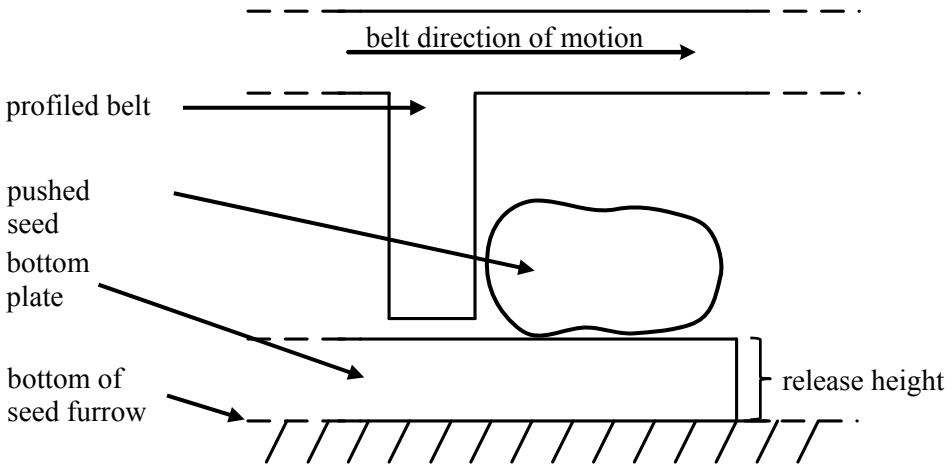

Figure 28. The release height is minimized by placing the mechanism as close to the ground as possible. The bottom plate sits directly on the ground in the seed furrow.

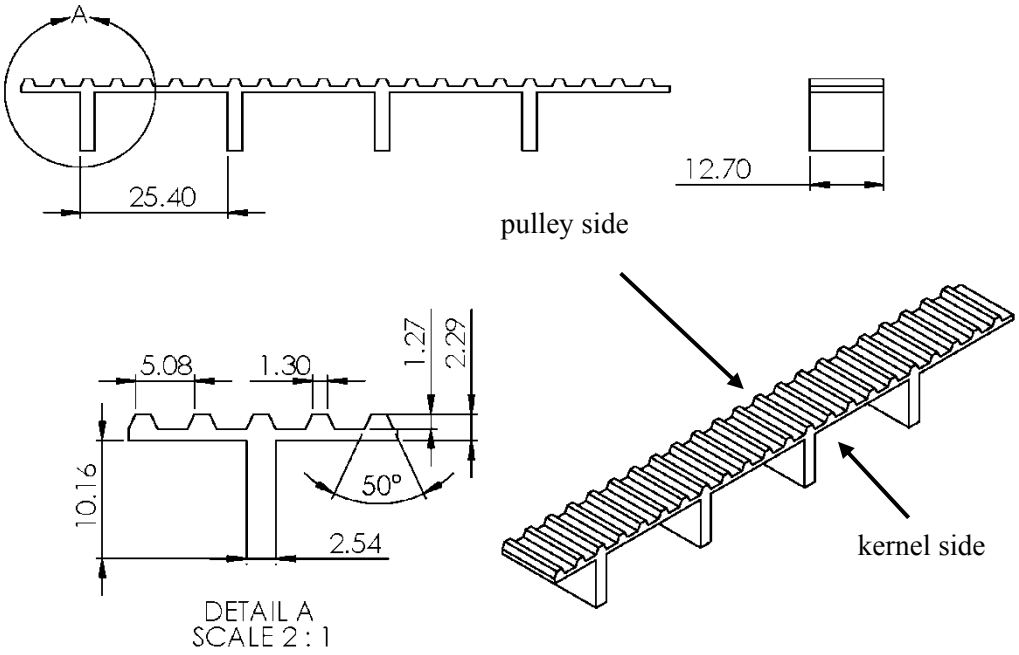

Figure 29. The belt design details were derived from the seed physical properties, the mechanism geometry, and the planting objectives.

Considering these results led to the belt design depicted Figure 29. The teeth pattern on the pulley side is a standard XL timing belt design for ease of compatibility with commercially available pulleys. The profiles on the kernel side were spaced about 25 mm apart on a belt roughly 12 mm wide. The profiles were kept narrow (2.5 mm) for good flexibility of the belt and about 10 mm tall to provide ample clearance for the seeds to first tumble into a flat orientation and then rotate. This belt design was custom manufactured by Belt Corporation of America, Cumming, GA (www.beltcorp.com).

Bench Test Setup

To validate the computational results based on analysis of 3D scans of corn seeds, the custom made profiled belt was installed in a wooden frame that was closed off at the bottom with a piece of Plexiglas to allow direct visual observation of the interaction between seed and belt. Of-the-shelf XL timing belt pulleys were installed such that the fully functional belt could be turned by hand. Spacers of 19 mm length were installed to provide clearance of about 3 mm between the belt and the sidewall on both sides. The setup is depicted in Figure 30.

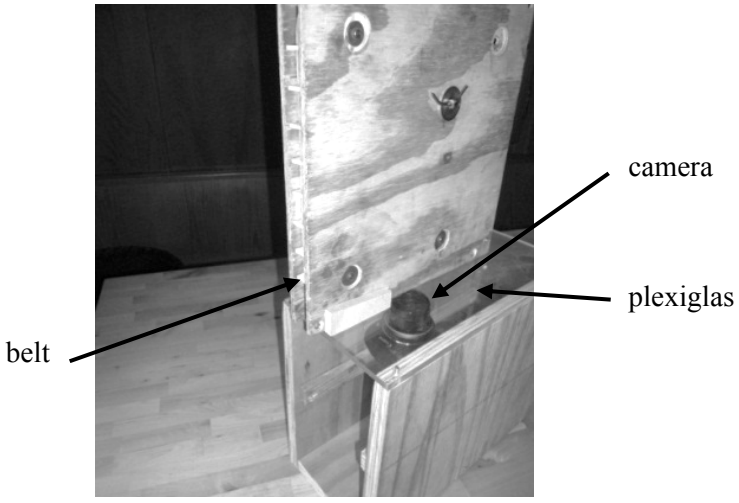

Figure 30. The bench test unit was closed off at the bottom with a piece of Plexiglas which allowed close observation of the seed orientation performance in the mechanism.

Sixty seeds of each hybrid were randomly selected from the same population as the scanned seeds and tested in the mechanism. The seeds were individually injected at one end and the drive pulley rotated to turn the belt. When the seed reached approximately the middle of the mechanism, a picture was taken from below through the Plexiglas with a digital camera. The angle of the seed with respect to the belt was measured in GIMP (Figure 32), an open-source image manipulation program (GIMP Development Team, 2013). The view depicted in Figure 32 is from below through the Plexiglas and the positive direction of the angular measurement is therefore reversed.

At this point, it becomes necessary to introduce an angular reference line relative to the belt. Since the belt is moving parallel to the furrow, this reference line is denoted furrow reference line. Its positive direction x_f points in the direction of planter forward motion, that is, the planting direction. This provides an unambiguous definition of the seed angle with respect to the belt. As shown in Figure 31, the reference line is chosen to be perpendicular to the pushing face of the belt tooth.

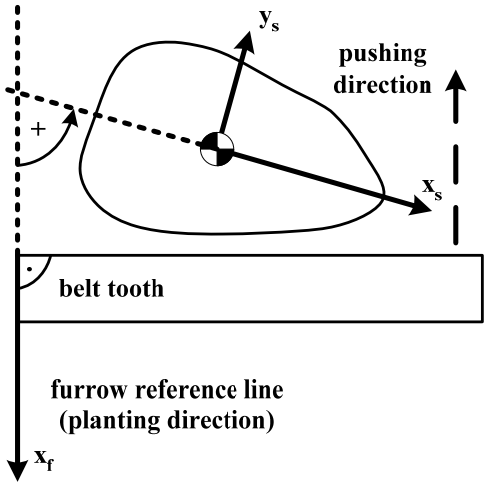

Figure 31. The angular reference line is perpendicular to the pushing face of the belt tooth and points in planting direction.

An angle of zero degrees is defined in the direction of x_f. Note that this is opposite to the direction of pushing. The orientation of the seed is measured from x_f to x_s in counterclockwise direction.

The angles are limited from 0 to ±180° (or 0 to ±π). By this definition the angle of the contact plane on the seed is of the same magnitude as the angle between x_f and x_s but of opposite sign.

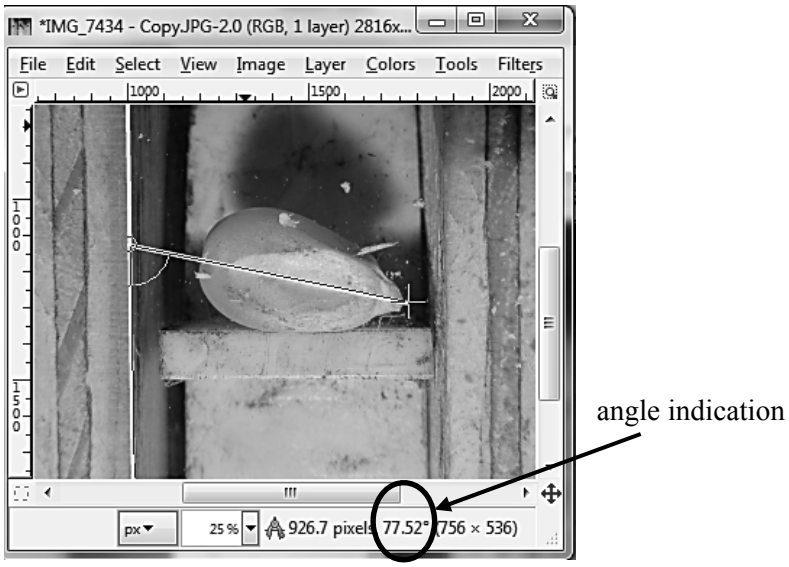

Figure 32. Angles were measurement in GIMP.

Results of In-Mechanism Orientation Measurements

Circular histograms for each hybrid were generated (Figure 33). The histograms are shown in the reference frame of the furrow. The 0°-direction points in the direction of planting which means that the belt moves from the right to the left as it pushes the seed. The figures show that the data obtained from the measurements in the mechanism matches very closely the computationally predicted orientation. As evident from Figure 33, the data was very clearly structured and was therefore separated along the predicted reversal points to obtain more statistical insight at the local stable points.

The analysis of the stable points, as summarized in Table 3, shows that the agreement with the prediction is excellent. This is emphasized in Figure 33, where the small triangles indicating the predicted mean kernel orientation for the different hybrids align very well with the measured data. The angular locations of the stable points predicted and measured differ only a few degrees.

The circular standard deviation is of the same order of magnitude. Some of the higher variability may be attributable to the experiment setup and measurement error. The seeds may be touching the sides as they are pushed along because the pushing plane is not of infinite length as assumed in the computational analysis. Furthermore, the accuracy of the measurements obtains from the image analysis may also be limited.

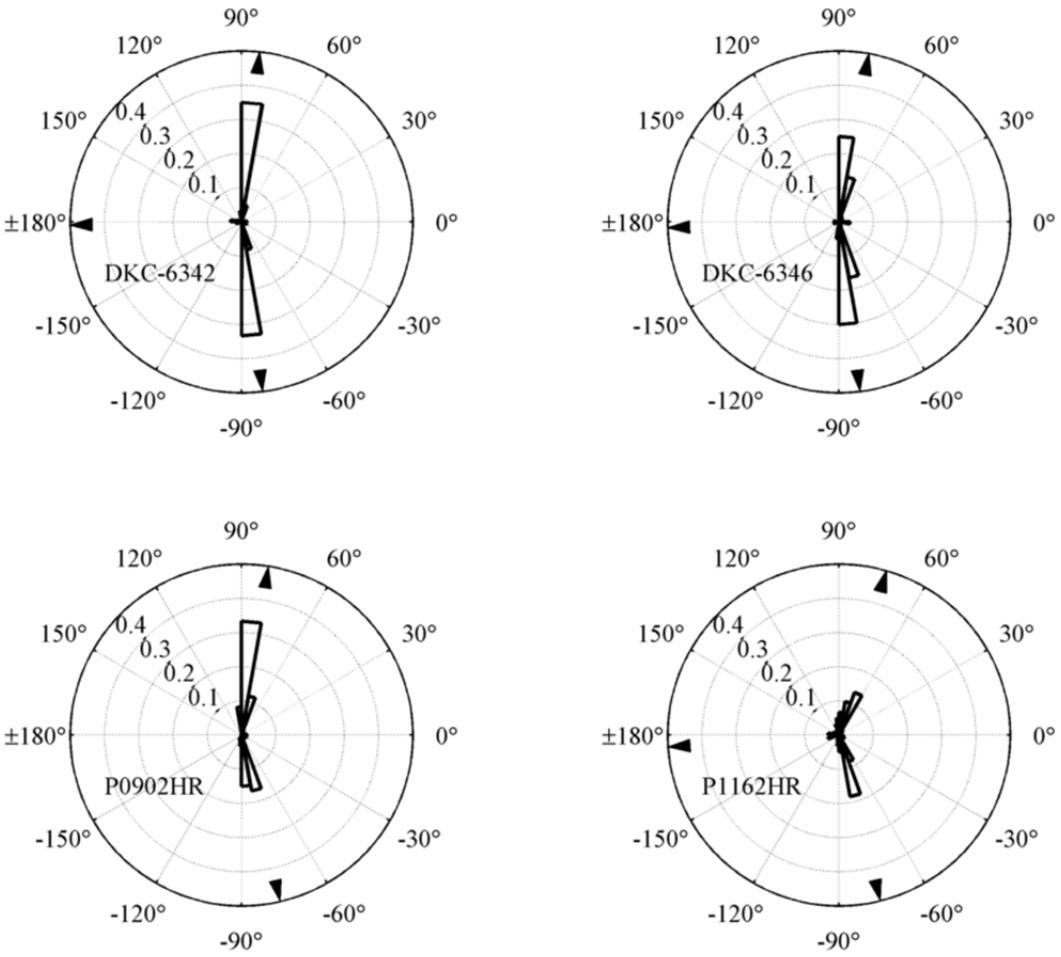

Figure 33. Histograms of the seed angles measured in the mechanism. The small triangles indicate the mean directions of the stable points found by computational analysis earlier.

The probabilities for the different final stable orientations were in good agreement with the prediction. However, the final orientations at SP_2 appear in the experiment with a much lower probability than predicted for all hybrids. This observation may be attributable to the fact that the

local minima at SP_2 are generally fairly weak. Slight disturbances of the center of friction by the above described rapid transition between support tripods may be sufficient to escape that local attraction point and diverge to one of the stronger local minima at either SP_1 or SP_3. For better readability and comparability, the angles in Table 3 have been converted to degrees and limited to ±180 and transferred into the reference frame of the seed (reversal of the sign as described above).

Hybrid	$SP_1[\mu°]^+$	$P(SP_1)$	$SP_2[\mu°]^+$	$P(SP_2)$	$SP_3[\mu°]^+$	$P(SP_3)$
DKC-6342						
predicted	84±6.1	0.42	-179±6.5	0.15	-83±4.6	0.43
measured	83±7.7	0.43	178±16.1	0.09	-76±6.1	0.48
DKC-6346						
predicted	80±6.9	0.40	-178±7.9	0.20	-83±10.2	0.40
measured	80±11.5	0.40	-175±14.5	0.04	-78±35.6	0.56
P0902HR						
predicted	81±13.9	0.50	n/a	n/a	-77±11.4	0.50
measured	81±28.2	0.57	n/a	n/a	-77±39.0	0.43
P1162HR						
predicted	74±11.8	0.34	176±21.0	0.31	-76±22.4	0.35
measured	76±32.7	0.43	174±31.7	0.13	-71±42.8	0.44

$^+$95% confidence intervals

Table 3. Comparison between predicted and measured orientation performance for the bench unit experiments.

Summary of Conceptual Analysis and Model Validation

The work presented in this chapter showed that the seed orientation may be achievable by pushing the kernels with a straight edge along a liner direction. Fifteen scanned kernels of 4 different hybrids of "medium flat" grading were computationally analyzed based on pushing and sliding models. The naturally variable kernels were systematically reduced to convex polygons to allow a pushing analysis in the plane. The highly simplified model produced very consistent results. Stable orientations at roughly ±80 degrees for each kernel could be computationally

identified. These stable points could be verified in measurements in a bench unit with a profiled belt to force the seeds along to achieve alignment with the pushing plane.

References

Brost, R. C. 1985. *Planning robot grasping motions in the presence of uncertainty*. Carnegie-Mellon University, The Robotics Inst itute.

Brost, R. C. 1988. Automatic grasp planning in the presence of uncertainty. *The International Journal of Robotics Research* 7(1):3-17.

Coskun, M. B., I. Yalcin, and C. Ozarslan. 2006. Physical properties of sweet corn seed (Zea mays saccharata Sturt.). *Journal of Food Engineering* 74(4):523-528.

GIMP Development Team. 2013. GIMP - GNU Image Manipulation Program, Release 2.8. Available at: http://www.gimp.org/. Accessed January 20, 2013.

Goldberg, K. Y. 1993. Orienting polygonal parts without sensors. *Algorithmica* 10(2):201-225.

Isik, E., and N. Izli. 2007. Moisture dependent physical and mechanical properties of dent corn (Zea mays var. indentata Sturt.) seeds (Ada-523). *American Journal of Food Technology* 2(5):342-353.

Jayan, P., and V. Kumar. 2004. Planter design in relation to the physical properties of seeds. *Journal of Tropical Agriculture* 42(1):69-71.

Kuehnle, J., A. Verl, X. Zhixing, S. Ruehl, J. M. Zoellner, R. Dillmann, T. Grundmann, R. Eidenberger, and R. D. Zoellner. 2009. 6D object localization and obstacle detection for collision-free manipulation with a mobile service robot. In *International Conference on Advanced Robotics.*

Lee, S. G., B. K. A. Ngoi, S. W. Lye, and L. E. N. Lim. 1996. An Analysis of the Resting Probabilities of an Object with Curved Surfaces. *International Journal of Advanced Manufacturing Technology* 12:366-369.

Lynch, K. M. 1999a. Inexpensive conveyor-based parts feeding. *Assembly Automation* 19(3):209-215.

Lynch, K. M. 1999b. Toppling manipulation. In *Robotics and Automation, 1999. Proceedings. 1999 IEEE International Conference on*. IEEE.

Mason, M. T. 1982. Manipulator grasping and pushing operations.

Mitchell, J. 2011. Vibratory tray feeders: Ten common problems and how to fix them. In *White Paper by Eriez Manufacturing Corporation*. CSC Publishing, Powder and Bulk Engineering.

O'Rourke, J. 1998. *Computational Geometry in C*. Cambridge University Press, New York.

Peshkin, M. A., and A. C. Sanderson. 1986a. Manipulation of a sliding object. IEEE.

Peshkin, M. A., and A. C. Sanderson. 1986b. The Motion of a Pushed, Sliding Object (Part 2: Contact Friction). *Robotics Inst., Carnegie-Mellon Univ., TR*:86-87.

Peshkin, M. A., and A. C. Sanderson. 1988. The Motion of a Pushed, Sliding Workpiece. *IEEE Transactions on Robotics and Robotics* 4(6):569-598.

Singh, S., M. Finner, P. Rohatgi, F. Buelow, and M. Schaller. 1991. Structure and mechanical properties of corn kernels: a hybrid composite material. *Journal of materials science* 26(1):274-284.

The MathWorks Inc. 2011. MATLAB 7.13 (2011b). *Natick, MA*.

Torralba, A., K. P. Murphy, W. T. Freeman, and M. A. Rubin. 2003. Context-based vision system for place and object recognition. In *Computer Vision, 2003. Proceedings. Ninth IEEE International Conference on*.

CHAPTER III

PHASE II: PROTOTYPE DEVELOPMENT AND TESTING

The objective of Phase II entailed the extension of the seed orientation concept from the bench test unit into a prototype system that could be deployed to the field. This chapter starts out by describing the design of the planter testbed. The prototype was then initially tested in laboratory setting and later under field conditions. The discovery of the importance of the relative velocity between seed and ground is discussed in detail. The field performance is first assessed based on the azimuth distributions of the seed leaves. Then the feasibility of an indirect post-emergence seed orientation performance assessment is discussed.

Prototype Design

The seed orientation concept was integrated into an existing John Deere Max Emerge row unit (John Deere Co., 2013b). A Computer Aided Design (CAD) model was initially developed in AutoDesk Inventor (Autodesk Inc., 2013) to facilitate the integration work. The subassembly breakdown of the planter prototype is depicted in Figure 34.

An ASABE Category 1 hitch interface (ASABE, 2007) was designed onto a short piece of 178 by 178 mm square tubing, serving as the toolbar. The row unit, complete with depth gauge wheel and furrow closing wheels, was then attached to the toolbar by suitable square U-bolts making the assembly an independent one-row planter testbed (Figure 35). A tray was installed above the toolbar to accommodate and support the power generator and control electronics.

The standard vacuum metering system including the seed hopper was left in place. Since no ground drive wheel was implemented, the vacuum meter and the orientation mechanism were driven by two independently controlled SureStep stepper motors (AutomationDirect.com, 2012). An E14 Series Dynapar (2013) encoder with 200 pulses per revolution was attached to one of the depth gauge wheels to provide a forward velocity estimate.

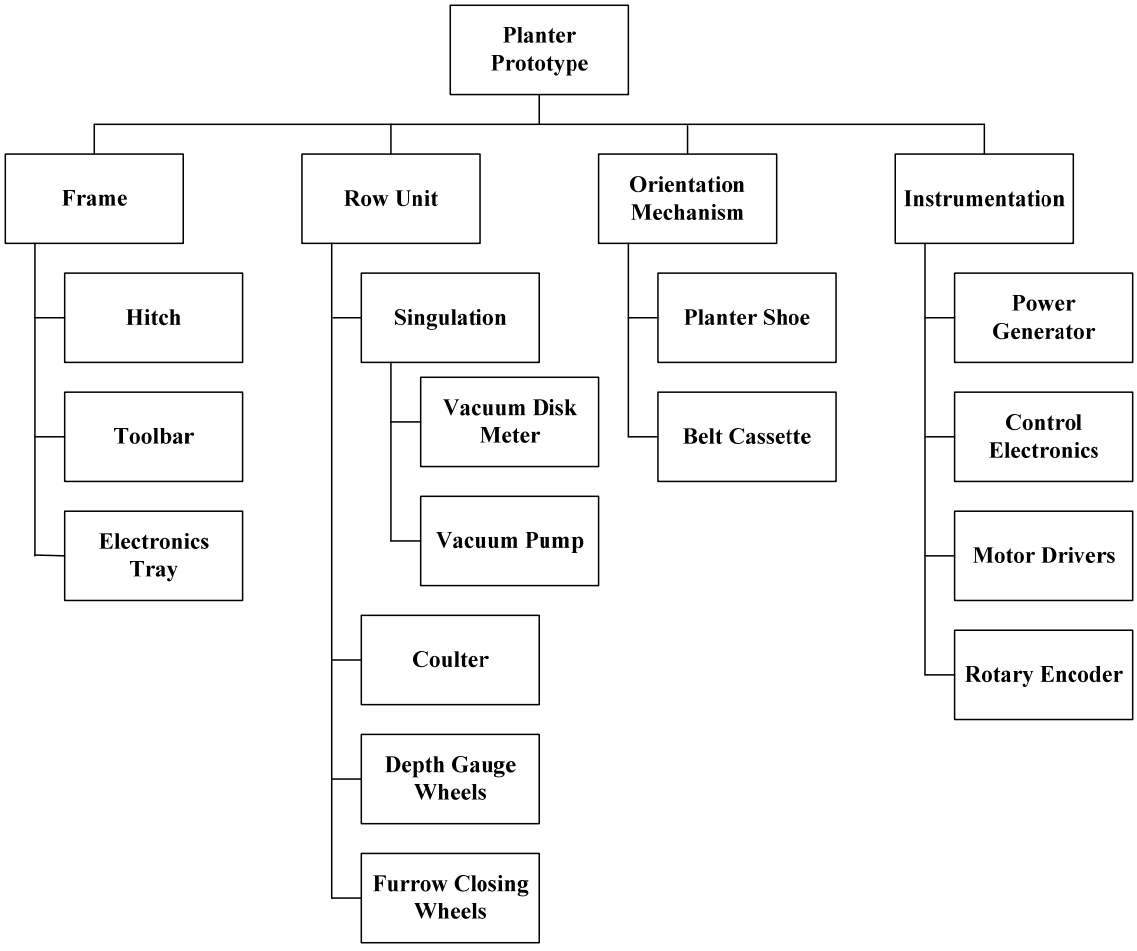

Figure 34. The subassembly breakdown of the planter prototype.

Figure 35. The prototype one-row planter in the field.

A VFC200-5T pump (Fuji Blowers, 2013) provided the necessary vacuum level for the singulation system. A vacuum gauge directly attached to the singulation housing indicated the vacuum level which was adjustable by a bleed valve in the vacuum supply line.

The standard disc openers were removed from the row unit because these discs cut a v-shaped furrow that does not allow the seed to lie flat. A MaxEmerge XP Runner Opener (John Deere Co., 2013a) was integrated instead. As shown in Figure 36, the rear of the runner was shortened and directly joined with the cassette containing the profiled belt. Only existing interfaces (holes, mounting stubs) on the row unit were used. Along the longitudinal axis of the planter, the runner opener was positioned such that the standard depth gauge wheels could be reused. Furthermore, runner and cassette were joined in such a way that the slightly shortened standard seed tube would feed directly into the inlet of the orientation mechanism. The cassette was designed to be as long as possible, limited by the requirement that the aft closing wheel mounting interface and functionality would not be obstructed or inhibited. The motivation for a long cassette was to provide ample space for the seed to slide and properly orient itself.

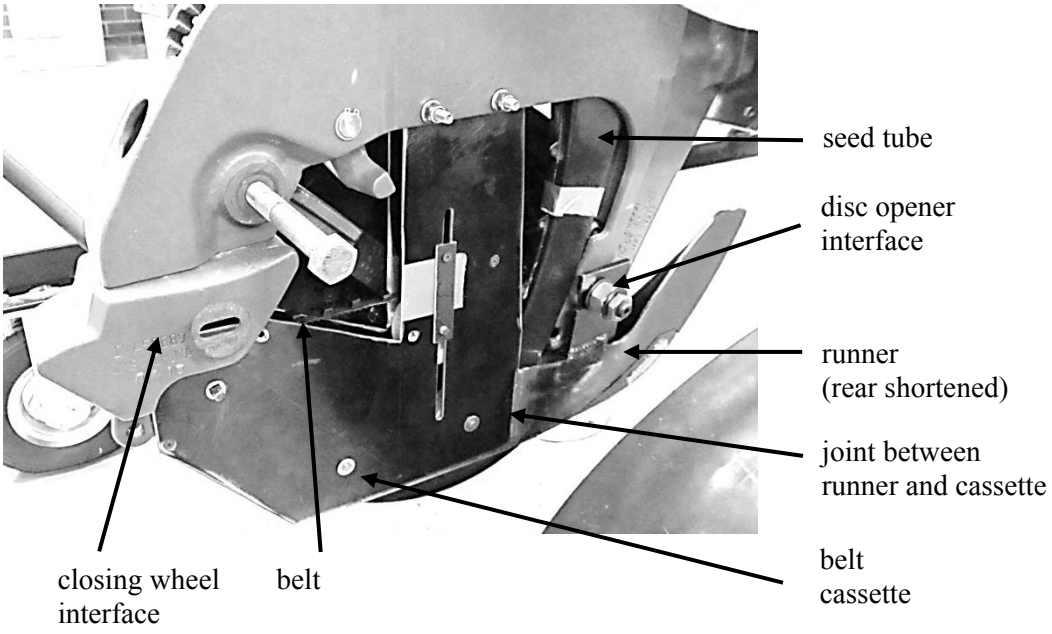

Figure 36. The runner opener was shortened and directly joined with the cassette containing the profiled belt.

The speed control of the singulator and the belt was implemented in C on an Arduino UNO, "an open-source electronics prototyping platform" (Arduino, 2013). The open-loop control concept is depicted in Figure 37 and the code run on the Arduino board is listed in Appendix A.

The incremental rotary encoder was sampled at 10 Hz and the signal filtered through a 2-pole Chebychev digital low-pass filter with a cutoff frequency of 1 Hz (Smith, 1997, p. 336). The application of the sensor scale factors to the filtered sensor data yielded the ground speed estimate. Including target seed spacing and the desired relative velocity between the seed and the ground enabled the computation of the stepping frequency for the singulator and belt motors, respectively.

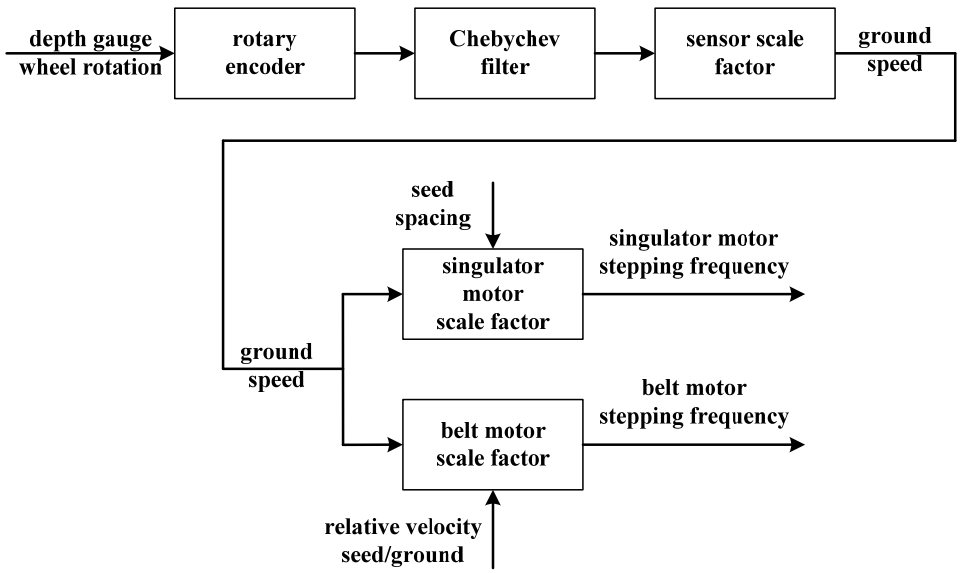

Figure 37. The speeds of both the singulator motor and the belt motor were individually controlled relative to the ground speed which was estimated based on a rotary sensor attached to the depth gauge wheel.

Control of Relative Velocity between Seed and Ground

Initially coupled by direct mechanical drive, it became quickly apparent during early tests that the speeds of the singulation unit and the belt must be individually controlled. Close observation by high-speed video revealed that the seed approached the release point inside the orientation mechanism oriented as expected from the results of the bench tests. However, the relative velocity between the seed and the ground at the time of the transition resulted in an unpredictable orientation change.

The entire system was originally driven by one motor, the speed of which was dictated by the required seed spacing. The mechanical coupling between the singulation disc and the belt was initially designed such that the advancement of one cell on the plate would result in the advancement of one cavity on the belt. Since the cavities were about 25 mm apart at the release point the seed would move at 25% ground speed with 100 mm target spacing, and only 10% ground speed with 250 mm spacing. The large acceleration of the seed when coming in contact

with the furrow bottom destroyed any angular alignment previously attained inside the mechanism. The relative velocity between the seed and the ground at the time of the transition from the mechanism to the furrow greatly influences the seed orientation performance. The design short-coming was improved by the implementation of independent belt speed control by a separate motor unit. As depicted in the control schematic in Figure 37, the stepping frequency of the singulator motor was then a function of the required seed spacing and the estimated ground speed. The stepping frequency of the belt motor was a function of ground speed only. To investigate the effect of ground speed to seed speed mismatch, the relative velocity factor r_v defined as the ratio between the seed velocity and the ground velocity was introduced.

Soil Bin Tests

The planter performance was assessed at laboratory conditions in a soil bin. In the subsequent tests, the planter was operated with retracted furrow closing wheels. The plywood soil bin depicted in Figure 38 was 4.5 m long, 0.45 m wide and 0.15 m high and was filled with a lightly packed sandy clay loam, a common soil type in Oklahoma. The soil was kept reasonably moist so that the furrow would remain open after the pass and prevent the furrow walls from crumbling and disturbing seeds. After a planting pass had been completed, a picture of each seed was taken with a digital camera (Figure 40) and so one pass produced about 15 to 20 measureable seeds depending on the selected seed spacing. Each treatment was repeated at least three times, resulting in a total of roughly 900 seeds that were planted and measured in the soil bin. The images were again analyzed using GIMP.

Effect of Relative Velocity between Seed and Ground on Orientation Performance

The objective of the first set of experiments was to investigate the effect of relative velocity between the seed in the orientation mechanism and the ground. The target seed velocity was computed by applying the relative velocity factor r_v to the ground speed. The data were then

collected according to the test parameters listed in Table 4. The hybrids, P0902HR and DKC-6346 were tested at six values of r_v ranging from 0.8 to 1.4. Data of a total of 36 passes were collected in the soil bin, yielding at least 50 measured seeds per treatment.

Factor	**Values**
hybrid:	[P0902HR, DKC-6346]
relative velocities factors (r_v):	[0.8, 0.9, 1.0, 1.1, 1.2, 1.4]

Table 4. The test parameters to investigate the relative speed effects.

Figure 38. The planter testbed was run in a soil bin for initial performance assessment.

The circular histograms of the raw data are depicted in Figure 39 for the hybrid P0902HR and in Figure 41 for the hybrid DKC-6346. Planter "forward" was in the direction of 0 degrees. As evident from the figures the performance at the two extreme measurement points at $r_v = 0.8$ and $r_v = 1.4$ appear little different from random orientation. The orientation performance at r_v closer to parity seems non-uniform with biases towards the desired across-row orientation. The preliminary

graphical assessment was complemented with a statistical investigation of which the results are summarized in Table 5. Each sample was tested for uniformity using the V-test. The uniformity hypothesis could not be rejected for $r_v = 0.8$ for both hybrids and for $r_v = 1.4$ for P0902HR. For the hybrid DKC-6346 with $r_v = 0.9$ the uniformity hypothesis was rejected but the estimation procedure for the von Mises parameters did not converge which is an indication that the non-uniformity was not strong enough.

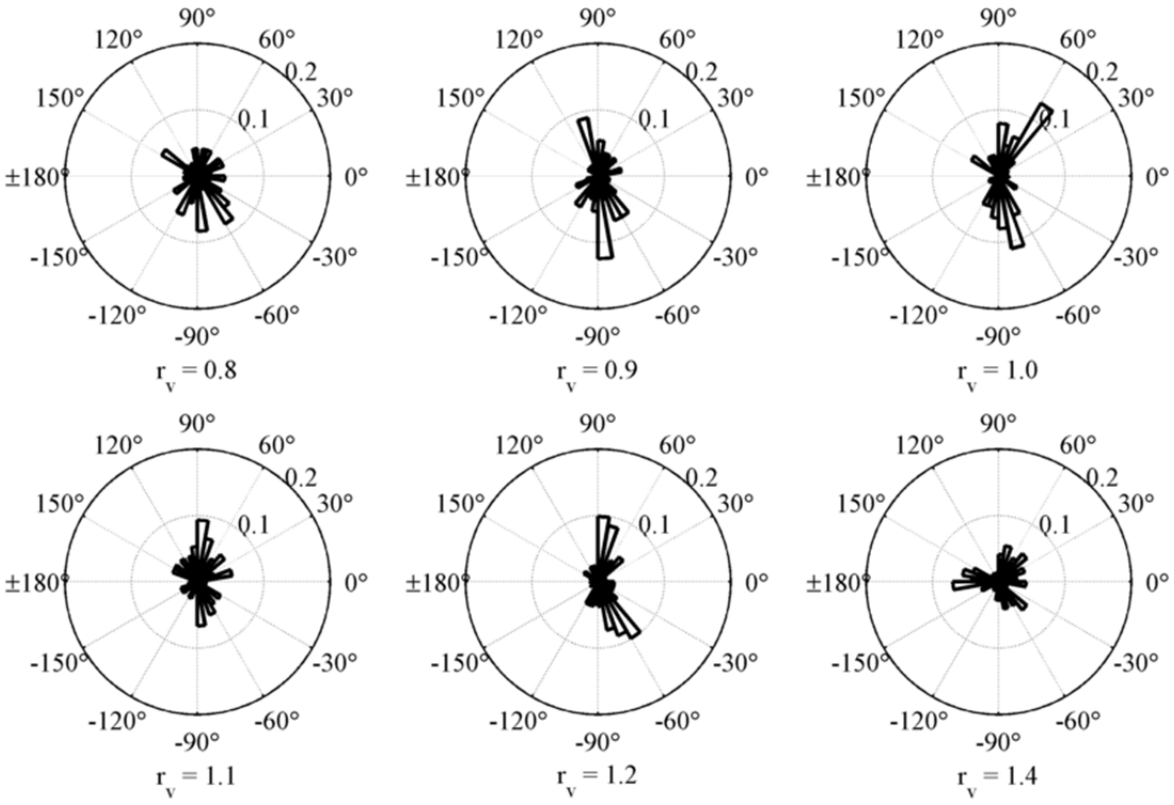

Figure 39. The orientation performance in the soil bin experiments for the hybrid P0902HR for different relative velocities between the seed and the ground at the release point.

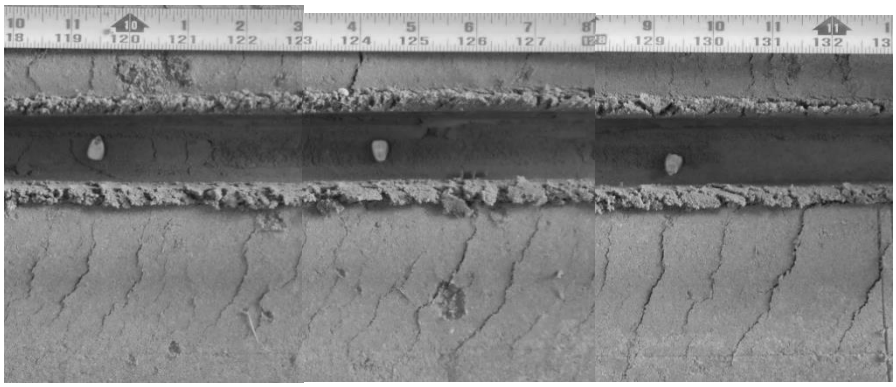

Figure 40. To measure the performance of the planter in the soil bin, pictures were taken with a digital camera and analyzed with GIMP.

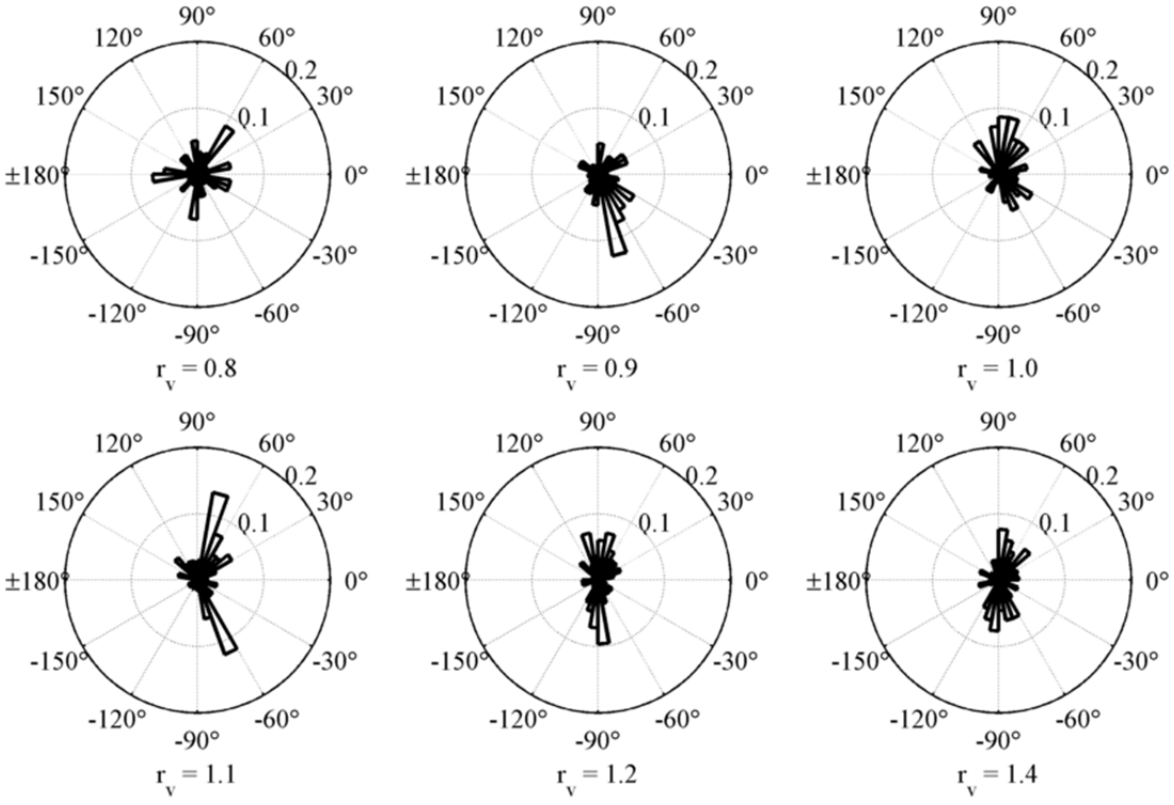

Figure 41. The orientation performance in the soil bin experiments for the hybrid DKC-6346 for different relative velocities between the seed and the ground at the release point.

P0902HR	μ_1[°]$^+$	κ_1[-]	μ_2[°]$^+$	κ_2[-]	% (μ_1, κ_1)
predicted	81±13.9		-77±11.4		
r_v = 0.8			n/a**		
r_v = 0.9	88.7±16.4	2.5	-81.2±11.8	3.5	43.8
r_v = 1.0	73.3±11.0	3.7	-84.2±7.7	7.5	53.1
r_v = 1.1	88.5±16.1	1.6	-68.6±16.9	2.4	66.7
r_v = 1.2	77.3±10.4	3.8	-64.8±8.8	4.2	44.4
r_v = 1.4			n/a**		

DKC-6346	μ_1[°]$^+$	κ_1[-]	μ_2[°]$^+$	κ_2[-]	% (μ_1, κ_1)
predicted	80±6.9		-83±10.2		
r_v = 0.8			n/a**		
r_v = 0.9			n/c*		
r_v = 1.0	78.4±8.7	6.1	-46.1±26.8	1.1	42.9
r_v = 1.1	67.3±13.1	2.2	-65.4±7.8	10.4	68.4
r_v = 1.2	78.1±12.2	2.4	-88.2±9.8	4.2	56.9
r_v = 1.4	72.7±15.4	2.2	-81.7±10.8	4.1	52.3

n/a**: uniformity hypothesis upheld; n/c*: non-converging parameter estimation; $^+$95% confidence

Table 5. Parameters of the von Mises mixtures were estimated for each non-uniformly distributed sample.

Although the computational investigations in Phase I have shown that there should be three stable resting orientations associated with DKC-6346, only a bimodal von Mises model was fitted. As the bench unit tests later in Phase II showed, the probability of the orientation SP_2 occurring is much lower in reality than predicted and is was therefore omitted in these models here. Hence, it was assumed that all data collected in the context of the soil bin experiments could be described by a model involving a mixture of two von Mises distributions.

Table 5 lists the estimated mean directions as well as the associated concentration parameters for the mixtures of two von Mises distributions. Note, that the separability into two modes by inspection of the data was not possible because the histograms are not as clearly structured as they were for the data of the bench unit tests. Therefore, a procedure described by Fisher (1996, pp. 97-98) was applied to obtain confidence intervals on the estimated mean directions. There is generally a very good agreement between prediction and measurement-based estimation of the mean direction. Comparison with Table 3 shows that the variability introduced through the

transition from the orientation mechanism to the ground increases the range of the 95%-confidence intervals of the mean directions. For P0902HR the measured mean directions are located on both sides of the prediction directions. However, the measured mean directions of the hybrid DKC-6346 appears biased towards with-row orientation.

There is no clear trend as to which value of r_v produces the best seed orientation performance. Clearly, test results with values of r_v too far from parity show that seed orientation is not transferred during placement, indicating that the difference between the seed velocity and the ground speed must be kept small at the time of the seed release. For the hybrid P0902HR the orientation performance appears to be best for speed parity. The concentration parameters of the two mixed von Mises models are the highest and the mean directions are only a few degrees from the prediction. For the hybrid DKC-6346 no stark trend is discernible from the data. These kernels appears to be more tolerant towards higher values of r_v since non-uniformity is still significant and parameter estimation is still converging at $r_v = 1.4$. Also, the concentration parameters remain high. However, this hybrid appears to be more susceptible towards lower values of r_v as parameter estimation for the samples with r_v less than parity was not possible.

Repeatability

The objective of a second set of experiments was to gauge the repeatability of the orientation. The 15 seeds of the hybrid DKC-6342 which were earlier sent for 3D scanning were run 12 times through the planter at $r_v = 1.2$. Since each seed was numbered, the measurement of each run could be assigned to a specific seed number and the seed-by-seed performance determined. The overall performance was assessed by combination of the data into one set as depicted in Figure 42. The circular histogram for the combination of all measurements looks similar to the ones obtained for the same value of r_v for the hybrids P0902HR and DKC-6346.

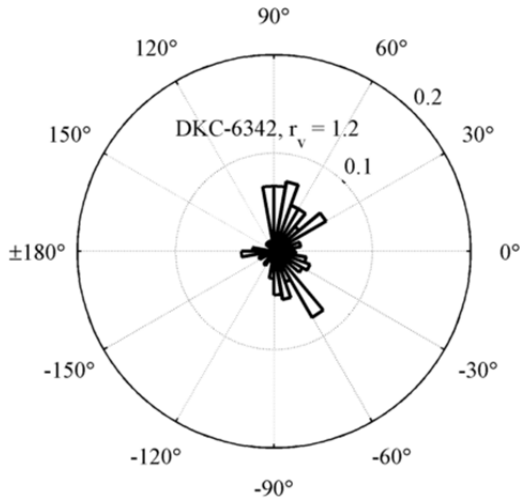

Figure 42. The combination of all repeatability measurements with kernels of DKC-6342.

Formal statistical assessment of the data, listed in Table 6, confirms this impression. The uniformity hypothesis is strongly rejected and the estimated parameters of the von Mises mixture show that the mean directions is again in the vicinity of the predicted values and the concentration parameters are high showing strong non-uniformity.

DKC-6342	**μ_1[°]**	**κ_1[-]**	**μ_2[°]**	**κ_2[-]**	**% (μ_1, κ_1)**
predicted	81		-77		
measured	68.7	3.9	-58.0	3.1	53.4

Table 6. Comparison between predicted and measured orientation performance.

However, the assessment of the orientation performance of each seed as an individual data set shows a different picture. The uniformity hypothesis is only rejected for eight seeds and only four of these actually allow parameter estimation for a von Mises mixture, for the other four seeds the parameter fitting does not converge. As evident from the listing in Table 7, the seeds for which the application of a von Mises model is possible show performance similar to the one measured for the hybrids P0902HR and DKC-6346. The comparison with the assessment of the combined

data set leads to the surmise that the sample size for the individual seeds are likely too small for more detailed conclusions.

DKC-6342	μ_1[°]	κ_1[-]	μ_2[°]	κ_2[-]	% (μ_1, κ_1)
predicted	81		-77		
Seed 1			n/c*		
Seed 2	51.5	4.4	-75.4	2.9	67.8
Seed 3			n/a**		
Seed 4	70.6	10.5	-30.3	1.66	37.1
Seed 5			n/a**		
Seed 6			n/c*		
Seed 7			n/a**		
Seed 8			n/c*		
Seed 9			n/c*		
Seed 10			n/a**		
Seed 11	58.1	4.3	-43.6	1.4	53.2
Seed 12	64.9	2.4	-62.4	4.1	26.3
Seed 13			n/a**		
Seed 14			n/a**		
Seed 15			n/a*		

n/a**: uniformity hypothesis upheld; n/c*: non-converging parameter estimation;

Table 7. The assessment of the individual seeds shows that only four seeds allow the fitting of parameters for a von Mises mixture.

In-Field Experiments

Upon completion of the soil bin tests, the planter was tested in the field. Rows at 0.75 m spacing and 22 m length were planted at Oklahoma State University's Agronomy Farm. The plot was watered and then tilled and smoothed before planting. The test parameters included the four hybrids, three relative velocity factors and the furrow closing wheels in retracted or engaged state (Table 8). The seeds were planted at 0.15 m spacing. Each treatment was planted twice. The trials of P1162HR at $r_v = 1.2$ could not be planted because the small amount of test seed available was depleted during the planting of the rows with $r_v = 0.8$ and $r_v = 1.0$. The rows planted with retracted furrow closing wheels were closed manually by hand after the planting pass. With the limitation on P1162HR discussed above, a total of 44 rows were planted.

Factors	Values
hybrid:	[DKC-6342, DKC-6346, P0902HR, P1162HR]
relative velocities factors (r_v):	[0.8, 1.0, 1.2]
closing wheels	[retracted, engaged]
seed spacing	[0.15 m]

Table 8. The test parameters for the field experiments.

In-Field Data Collection

When the collar of the seed leaf started forming, pictures of the emerged plants were taken in the field. As depicted in Figure 43, a digital camera was installed in a stand such that the stand could be aligned with the row and the resulting picture would be aligned with the row direction.

Figure 43. The pictures of the plants in the field were taken with a digital camera mounted to a custom stand.

At the beginning and the end of each row about 3 m were excluded from data recording. Images of roughly 2600 plants were recorded, yielding about 60 plants per row, that is, an average of about 120 data points per treatment. The seed leaf azimuth was then again determined in GIMP.

Results of In-Field Seed Orientation Performance Assessment

The circular histograms of the field data for the different treatments of the hybrid DKC-6346 are depicted in Figure 44. The data of all other hybrids are depicted in Appendix B. Inspection of the histograms does not reveal any immediately obvious concentration of the seed leaf azimuths at

the target orientations of ±90°. A formal V-test, as summarized in Table 9, provides a clearer picture. None of the treatments at $r_v = 0.8$ shows a seed leaf azimuth distribution that is significantly different from uniformly random.

The hybrid DKC-6342 shows significant non-uniform leaf azimuth distributions for $r_v = 1.2$, for configurations with and without closing wheels. DKC-6346 shows significant non-uniform random seed leaf azimuths for $r_v = 1.0$ and $r_v = 1.2$ but only with closing wheels. P0902HR and P1162HR show significant non-uniform random seed leaf azimuths for $r_v = 1.0$ but neither for $r_v = 1.2$ nor $r_v = 0.8$ and only for the configuration with engaged closing wheels. This may indicate that the closing wheels are a less disturbing process than furrow closing by hand.

These results confirm that the value of r_v is a crucial parameter in the performance of mechanized seed orientation. The findings also reiterate earlier conclusions that the hybrids DKC-6342 and DKC-6346 favor higher values of r_v. The lower significance values of P0902HR and P1162HR show that that the kernels of these two hybrids are in general less suitable for mechanized seed orientation.

	DKC-6342		**DKC-6346**		**P0902HR**		**P1162HR**	
V-test	no c.w.	with c.w.	no c.w.	with c.w.	no c.w.	with c.w.	no c.w.	with c.w.
$r_v = 0.8$	ns	ns	ns	ns	ns	ns	ns	ns
$r_v = 1.0$	ns	ns	ns	2.08^{+}	ns	1.71^{*}	ns	1.72^{*}
$r_v = 1.2$	1.69^{*}	2.14^{+}	ns	1.91^{**}	ns	ns		

*significant at 0.1, **significant at 0.05, $^{+}$significant at 0.01

Table 9. The results of the V-test for uniformity.

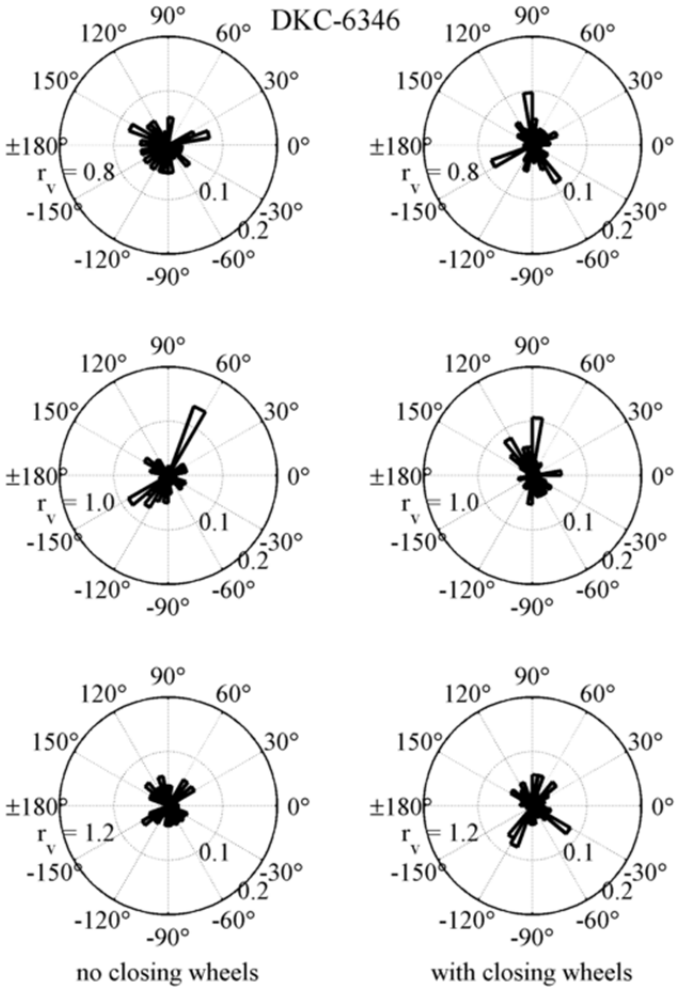

Figure 44. The circular histograms of the seed leaf azimuths for the different treatments of the hybrid DKC-6346.

Summary and Conclusions

The soil bin experiments, where direct seed orientation was measured, showed that mechanized seed orientation by pushing is possible, including the transition from the orientation mechanism to the ground. Control of the relative velocity between the seed and the ground at the time of the release was identified as a critical aspect. The relative velocity of the seed must be a least 1.0. A factor of 1.4 on other hand was measured to be too large. The best orientation results were obtained with relative velocity factors in the range of 1.1 to 1.2.

The field experiments allowed measurements of leaf azimuths only. Despite some natural variability between seed and leaf azimuth, it could be shown that the seed leaves for the hybrids DKC-6342 and DKC-6346 were non-uniformly distributed with preference across-row. The closing wheels have at least no obvious negative impact on the orientation performance.

References

Arduino. 2013. Arduino - An open-source electronics prototyping platform. Available at: http://arduino.cc/en/. Accessed February 23, 2013.

ASABE. 2007. Three-Point Free-Link Attachment for Hitching Implements to Agricultural Wheel Tractors. *ASAE S217.12 DEC2001 (ISO 730-1:1994) (R2007)*.

Autodesk Inc. 2013. Autodesk Inventor Products. Available at: http://usa.autodesk.com/autodesk-inventor/. Accessed February 22, 2013.

AutomationDirect.com. 2012. SureStep Stepping Systems User Manual - Fourth Edition 12/2012. Available at: http://www.automationdirect.com/static/manuals/surestepmanual/surestepmanual.html. Accessed February 22, 2013.

Dynapar. 2013. E14 | Miniature Encoder - Product Data Sheet. Available at: http://www.dynapar.com/Products_and_Solutions/Series_E14_Miniature_Encoder/. Accessed Feburary 22, 2013.

Fisher, N. I. 1996. *Statistical Analysis of Circular Data*. Cambridge University Press.

Fuji Blowers. 2013. VFC20 - Ring Compressor, Product Data Sheet. Available at: http://www.fujiblowers.com/pdfs/VFC20.pdf. Accessed February 20, 2013.

John Deere Co. 2013a. MaxEmerge, XP Runner Opener. Available at: http://salesmanual.deere.com/sales/salesmanual/en_NA/seeding/2012/feature/row_units_and_drill_opener/planters/xp_runner_story.html. Accessed.

John Deere Co. 2013b. Row Units. Available at: http://www.deere.com/wps/dcom/en_CAF/products/equipment/planting_and_seeding_equipment/planters/row_units/row_units.page. Accessed February 7, 2013.

Smith, S. W. 1997. *The Scientist and Engineer's Guide to Digital Signal Processing*. www.DSPguide.com.

CHAPTER IV

PHASE III: FEASIBILITY OF A POST-EMERGENCE SEED ORIENTATION PERFORMANCE MEASURE

The leaf azimuth is not deterministically coupled to the seed orientation. Although Torres et al. (2011) identified the principal seed orientations that produce preferentially across-row oriented leaves, there exists statistical variation from seed to seed. At the same time, the investigations above have shown that the seed orientation produced by the planter is subject to similar variability that may be described by statistical models. Hence, the observable leaf azimuth distribution is likely a combination of the two distributions, which can be described by convolution of two von Mises distributions. However, a convolution of two von Mises distributions is no longer a von Mises distribution. Nonetheless, as shown by Mardia and Jupp (2000, p. 44) a very good approximation is given by

$$\begin{aligned} & f_1(\theta_1;\ \mu_1, \kappa_1) * f_2(\theta_2;\ \mu_2, \kappa_2) \\ & \approx f_{12}\left(\theta_{12};\ \mu_1 + \mu_2, A^{-1}\left(A(\kappa_1)A(\kappa_2)\right)\right) \end{aligned} \tag{4.1}$$

where

$$A(\kappa_i) = \frac{I_1(\kappa_i)}{I_0(\kappa_i)} \tag{4.2}$$

with $I_i(\cdot)$ being the modified Bessel function of the first kind of order i. Obtaining $A^{-1}(\cdot)$ can be difficult but it is available in tabulated form, for example, in Fisher (1996).

So, if one of the two models could be identified and described, say, μ_1 and κ_1, the other component of the convolution could be isolated. Therefore, the proposed approach here is to measure f_{12} in the field and then use the model for the seed-to-leaf azimuth distribution f_1 to calculate the parameters of the in-field planter performance f_2.

However, to date, no statistical models of the correlation between seed and leaf azimuth exist. Drouet et al. (1999) and Maddonni et al. (2001) already documented that the leaves on a single plant obviously do not lie strictly in a plane but also exhibit variability in azimuth.

Seed Leaf as Seed Angle Indicator

Since the interaction between plants may influence leaf azimuth (Girardin and Tollenaar, 1994), it has been decided to select a very early leaf as indicator of the seed orientation before neighboring plants may affect each other's leaf azimuth distribution. Viewed from the top, the leaf should be visible without being obstructed by other leaves at the time of the measurement. Since a leaf's azimuth may change significantly until the formation of the leaf collar (Drouet and Moulia, 1997; Drouet et al., 1999), the measurement cannot be taken until the leaf collar is starting to set. However, at that same time, the next leaf may already start to overlap. The seed leaf has therefore been selected as the seed angle indictor.

Experiment Setup and Data Collection

Since the planter was designed to plant the seeds flat with either the embryo up or down, the investigations could be limited to these two orientations. Of each of the four hybrids 80 seeds were planted at the greenhouse of the Oklahoma State University Agronomy Farm: 40 seeds with embryo up, 40 seeds with embryo down. Each treatment was repeated three times, yielding a total of roughly 120 data points per treatment. Non-emergence rate was in the normal range of 2 to

3%. The seeds were placed in flower pots with reference markings, as depicted in Figure 45. The reference frame was defined such that the single tick represents the 90° direction and the triple tick the -90° direction for consistency with the results presented above. The row or planting direction can therefore again assumed to be in the direction of zero degrees. Before covering the seed with soil, a picture was taken of each pot with a digital camera mounted in a custom camera stand to ensure a perpendicular view from above (Figure 46).

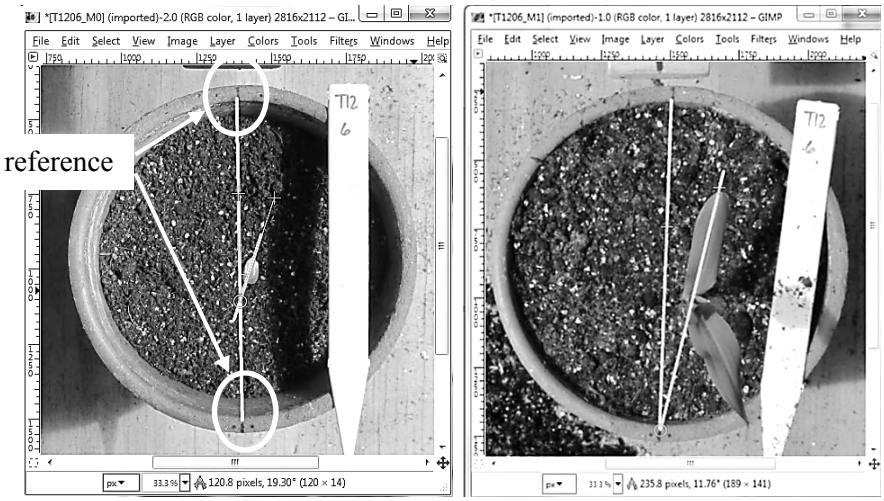

Figure 45. The seeds were planted in flower pots with references markings and the seed and the seed leaf angle measured with respect to these marking.

After emergence, a second picture was taken of the plant in the pot right at the time of leaf collar development on the seed leaf. The seed and seed angle were then then measured with respect to the reference markings in the image using GIMP once again.

Figure 46. All pictures throughout the experiment were taken with a digital camera mounted in a custom camera stand.

Fitting of von Mises Distribution Models

The circular histograms of the collected data confirm in general the findings documented by Torres et al. (2011). The two examined seed orientations, "flat, embryo up" and "flat, embryo down", result in non-uniform distributions of seed leaf azimuths. The mean direction may then be chosen to lie across the row with appropriate planting. However, when examining the circular histograms in Figure 47 through Figure 50 a surprising fact becomes immediately apparent: the orientation "embryo up" or "embryo down" cause the seed leaf to emerge in directions that are 180° opposite. As evident from the listing in Table 10, the mean seed leaf azimuths for the orientation "embryo up" is roughly 90° and for "embryo down" approximately -90°. As documented below, this effect has profound implications on the feasibility of post-emergence seed orientation performance assessment.

The fitting of von Mises parameters revealed that the concentration parameters for the hybrid DKC-6342 are generally the highest and the mean azimuth the closest to ±90° as desired. The orientation "embryo down" in general appears to lower the concentration parameters (not true for P1162HR).

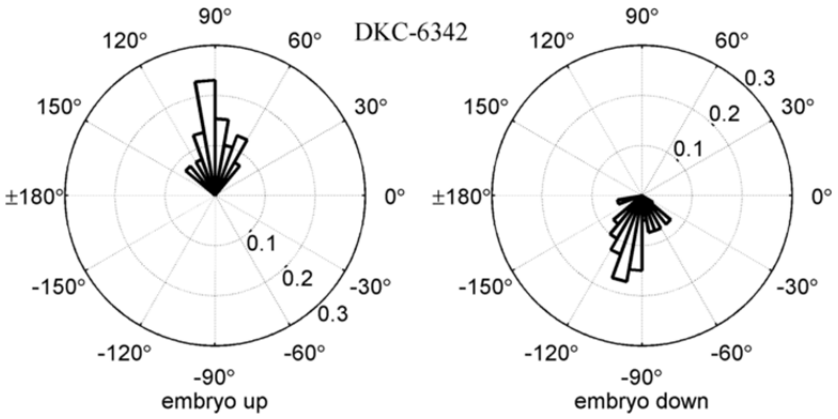

Figure 47. Measured seed leaf azimuths for the hybrid DKC-6342 for embryo up and down.

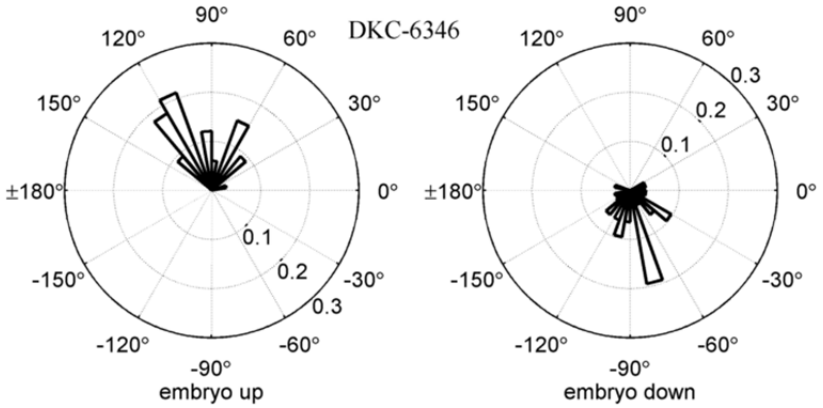

Figure 48. Measured seed leaf azimuths for the hybrid DKC-6346 for embryo up and down.

	embryo up				embryo down			
Hybrid	**μ[°]**	**κ[-]**	**U^2**	**U^2_{crit}***	**μ[°]**	**κ[-]**	**U^2**	**U^2_{crit}***
DKC-6342	90.7	7.7	0.056	0.113	-98.5	4.2	0.034	0.113
DKC-6346	96.1	3.8	0.101	0.111	-79.9	1.9	0.029	0.095
P0902HR	102.1	3.8	0.055	0.111	-104.5	1.7	0.047	0.093
P1162HR	98.8	2.6	0.032	0.105	-107.3	5.1	0.077	0.113

*α = 0.05

Table 10. The von Mises distribution model parameters (mean direction μ and concentration parameter κ) for the seed leaves with planting orientations "flat, embryo up" and "flat, embryo down".

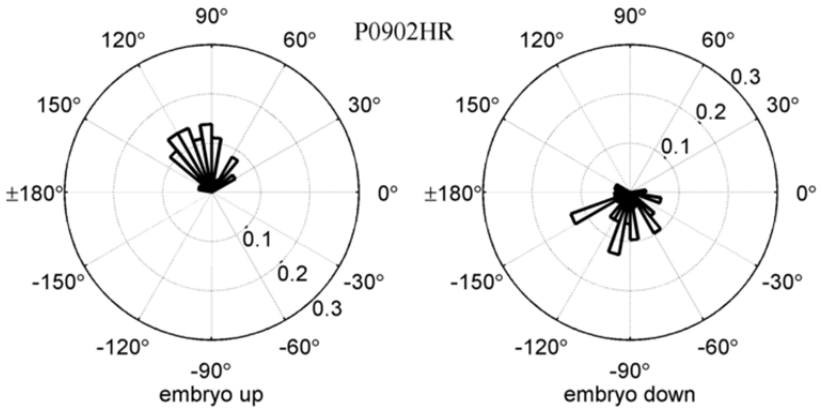

Figure 49. Measured seed leaf azimuths for the hybrid P0902HR for embryo up and down.

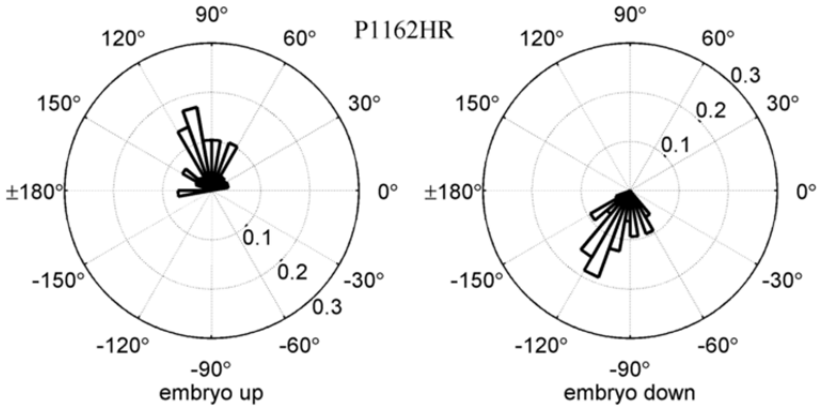

Figure 50. Measured seed leaf azimuths for the hybrid P1162HR for embryo up and down.

The U^2 goodness-of-fit test results collected in Table 10 confirm that the von Mises distribution is a good approach to modeling the seed leaf azimuth distribution with respect to the seed orientation.

The measured mean directions were then tested against the hypothesis if the mean direction was in fact statistically different from the anticipated mean direction of ±90. The test statistics E_n was computed according to Fisher (1996, p. 93):

$$E_n = \frac{\sin(\mu - \mu_0)}{\sigma_{vM}} \tag{4.3}$$

This value can be compared to the 100(1-0.5α)% percent points of the normal distribution.

	embryo up		embryo down	
Hybrid	**μ[°]**	**E_n***	**μ[°]**	**E_n***
DKC-6342	90.7	0.21	-98.5	1.77
DKC-6346	96.1	1.10	-79.9	1.11
P0902HR	102.1	2.29	-104.5	1.48
P1162HR	98.8	1.18	-107.3	3.58

*$\alpha = 0.05 \rightarrow E_{n,\,crit} = 1.96$

Table 11. The mean directions with E_n-test of the leaf azimuths for the hybrids DKC-6342 and DKC-6346.

As shown in Table 11, the estimated mean directions for the hybrids DKC-6342 and DKC-6346 cannot be determined to be different from the expected ±90°. However, the mean seed leaf direction for the hybrids P0902HR and P1162HR may be different from ±90 degrees. The value of E_n is generally higher for these two hybrids. Furthermore, embryo down may introduce a bias or at least higher variability, as indicated by larger values of E_n for almost all hybrids.

Comparison of Model Parameters

The models were then compared to evaluate if there is any evidence that seed leaf azimuth distribution for the different hybrids or seed orientation is statistically different. As discussed earlier, the methods require that the concentration parameters are compared before the differences between mean directions can be assessed.

In order to compare "embryo down" and "embryo up" orientations, the reference frame of the data of the latter was rotated by 180°. Table 12 shows the results of the comparison test of the concentration parameters with the orientation "embryo up" across the four different hybrids. While the notion of equal concentration for DKC-6342 and the three other hybrids is (nearly) consistently rejected, the differences between DKC-6346, P0902HR, and P1162HR appear negligible.

The comparison of the concentration parameters for the "embryo down" orientation is collected in Table 13. Equality of the concentration parameters for the orientation "embryo down" is rejected for all pairs except between DKC-6346 and P0902HR, and between DKC-6342 and P1162HR. The result that the concentration parameters of DKC-6342 and P1162HR cannot be deemed different is somewhat unexpected. However, a comparison of the "embryo down" circular histograms in Figure 47 and Figure 50 shows that, in fact, the observed measurements are nearly identical.

κ, "up"	**DKC-6346**		**P0902HR**		**P1162HR**	
	F	**F_{crit}***	**F**	**F_{crit}***	**F**	**F_{crit}***
DKC-6342	6.82	3.97	2.98	3.97	6.47	3.98
DKC-6346			0.35	3.98	0.13	3.99
P0902HR					0.73	3.99

*α = 0.05

Table 12. Comparison of the concentration parameters of the von Mises models of the different hybrids for the seed orientation "embryo up".

κ, "down"	**DKC-6346**		**P0902HR**		**P1162HR**	
	F	**F_{crit}***	**F**	**F_{crit}***	**F**	**F_{crit}***
DKC-6342	5.25	3.97	6.42	3.97	0.12	3.97
DKC-6346			0.08	3.99	6.46	3.99
P0902HR					7.53	3.99

*α = 0.05

Table 13. Comparison of the concentration parameters of the von Mises models of the different hybrids for the seed orientation "embryo down".

The results of the cross-comparison between "embryo up" and "embryo down" are listed in Table 14. Interestingly, the cross-comparison only shows a significant difference of the concentration parameters between four pairs. One notable observation is P0902HR which is the only hybrid where the concentration parameter between "embryo up" and "embryo down" is calculated to be

different. Since the results are not conclusive for either equality or inequality of the concentration parameters, it must be assumed they are not equal until these results may be refined by additional data.

κ "embryo up"	"embryo down" DKC-6342		DKC-6346		P0902HR		P1162HR	
	F	F_{crit}*	F	F_{crit}*	F	F_{crit}*	F	F_{crit}*
DKC-6342	2.62	3.96	15.71	3.97	17.06	3.97	1.56	3.97
DKC-6346	0.63	3.97	2.56	3.99	3.43	3.99	1.33	3.99
P0902HR	0.02	3.96	4.15	3.99	5.16	3.98	0.23	3.98
P1162HR	1.09	3.98	1.07	4.00	1.62	4.00	1.73	4.00

*α = 0.05

Table 14. The results of the cross-orientation comparison of the concentration parameters.

With the concentration parameters not all equal, the Y-test for differences in mean directions as described in Fisher, 1996, p.124 was applied to the data. The critical value for a one-on-one comparison at α=0.05 is 3.84. The calculated results are summarized in Table 15, Table 16, and Table 17. The results show that with "embryo up", the mean directions are essentially equal because no significant difference could be detected. For seed orientation "embryo down" the mean directions between DKC-6346 and P0902HR and DKC-6346 and P1162HR appear to differ.

μ, "up"	DKC-6346 Y	P0902HR Y	P1162HR Y
DKC-6342	0.69	3.31	0.98
DKC-6346		0.61	0.08
P0902HR			0.13

*α = 0.05, Y_{crit} = 3.84

Table 15. Comparison of the mean directions of the von Mises models of the different hybrids for the seed orientation "embryo up".

μ, "down"	DKC-6346 Y	P0902HR Y	P1162HR Y
DKC-6342	3.28	0.31	1.74
DKC-6346		3.44	7.12
P0902HR			0.66

*$\alpha = 0.05$, $Y_{crit} = 3.84$

Table 16. Comparison of the mean directions of the von Mises models of the different hybrids for the seed orientation "embryo down".

When comparing "embryo up" and "embryo down" in Table 17 the hybrids DKC-6342 and P1162HR appear not to agree very well with the other two hybrids. In the cross-comparison in Table 17, the diagonal entries are of particular interest. These results indicate agreement or disagreement between the mean direction of "embryo up" and "embryo down" in one particular hybrid. While the DKC-6342 and DKC-6346 show no difference in mean direction, the equality of the mean direction between "embryo up" and "embryo down" cannot be assumed for P0902HR and P1162HR. For these two hybrids this may indicated that the offset between the mean seed leaf azimuth of a seed planted with the embryo down and one which was placed with embryo up is in fact different from 180°.

μ	"embryo down"			
"embryo up"	DKC-6342 Y	DKC-6346 Y	P0902HR Y	P1162HR Y
DKC-6342	2.46	0.93	2.19	9.46
DKC-6346	3.99	0.13	3.41	10.27
P0902HR	8.43	0.03	5.80	17.16
P1162HR	3.84	0.01	3.65	8.74

*$\alpha = 0.05$, $Y_{crit} = 3.84$

Table 17. The results of the cross-orientation comparison of the mean directions.

Summary and Conclusions

In the context of the greenhouse experiments, three key discoveries were made.

1. The long-axis of the seed may be used as a reference direction. The emerging seed leaf azimuths are centered at and distributed around the reference direction.

2. “Embryo up” and “embryo down” seed orientation produce seed leaf azimuths at 180° offset.
3. The seed leaf azimuth distribution may be modeled by a von Mises distribution.

However, at this point the data is inconclusive as to whether or not the seed leaf azimuth distribution can be described by a *unified von Mises model* across different hybrids. There are indications that different hybrids exhibit different behavior. If the seed leaf azimuth distribution can convincingly be shown to be a hybrid-specific property, genetic selection for favorable behavior may become necessary.

Furthermore, the observations associated with the hybrids P0902HR and P1162HR suggest that a more accurate prediction of the mean seed leaf direction may be possible if the reference direction x_s is chosen to be aligned with some other feature of the seed. For these two hybrids, the measured mean direction appears to be offset from the x_s-direction. A more in-depth investigation from a botanical point of view may be required. It may not be the orientation of the exterior shape that ultimately defines the seed leaf azimuth.

Identification of seed orientation performance parameters based on this data is clearly difficult to achieve. Separation of the data sets along modes into subgroups with subsequent isolated model fitting is impossible. It may therefore be helpful to review what has been discussed so far to understand the expected underlying structure of the measurements. In Phase I and II it was discovered that because of the exterior shape of the seed, in the best case the seed would be oriented at roughly 80° or, depending on the initial orientation, at about -80° with respect to the row direction. During greenhouse experiments with the hybrid seeds in Phase III it became obvious that that the azimuth of the seed leaf would depend strongly on whether the embryo was up or down at the time of planning. Since the resulting seed leaf azimuths are offset by 180°, this has severe implications for the post-emergence measurement: it implies that the combination of

four mean directions of seed leaf azimuths may be present in the data set. The fact that of the over 900 seeds measured during the soil bin experiments about 520 seeds were oriented “embryo up” and some 420 seeds “embryo down” supports the conclusion that “embryo up” and “embryo down” is about equally likely and that the four mean directions also equally likely occur. The predicted mean directions of the seed leaf azimuths would then be roughly ±80° and ±100. A pictorial representation is shown in Figure 51.

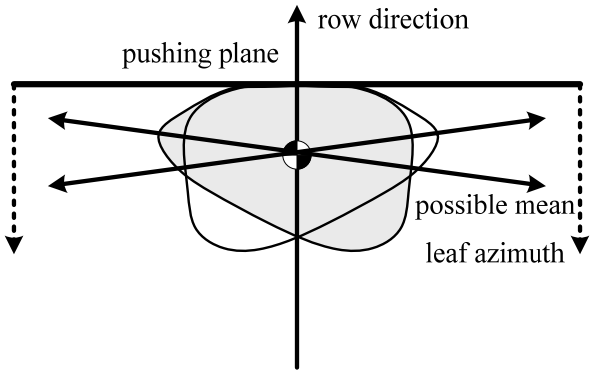

Figure 51. The fact that “embryo up” and “embryo down” produce seed leaves at 180° offset results in a mixture four mean directions being present in the seed leaf azimuth measurements.

Considering the quite small concentration factors present in the seed to leaf azimuth correlation discovered in the greenhouse experiments and factoring in the variability produced by the planter, it becomes very difficult to separate the data. For illustrative purposes, consider the hybrid DKC-6346. As determined by the greenhouse experiments, the seed leaves may be assumed to emerge at the mean directions of +90° and -90° if the seeds x_s-axis is perfectly aligned perpendicularly to the row direction (either embryo up or down). The concentration parameters of the emerging leaves have been determined to be 3.8 for seeds with embryo up and 1.9 for seeds with embryo down. However, as shown in Phase II, the seed’s exterior shape will cause it to take the measured average angles of roughly ±80° when planted by the orientation mechanism. Therefore,

considering no variability of the planter performance for the moment, the resulting seed leaf azimuth distribution can be expected to be a mixture of the following four models:

$$\theta_1 \sim \text{vM}(80, 3.8)$$

$$\theta_2 \sim \text{vM}(-80, 3.8)$$

$$\theta_3 \sim \text{vM}(100, 1.9)$$

$$\theta_4 \sim \text{vM}(-100, 1.9)$$

Figure 52 depicts the simulated seed leaf azimuth distribution for 120 leaves, a mixture of 30 randomly generated leaf azimuths of each of the above distributions. Notes on how to generate von Mises samples with given distribution parameters can be found in Fisher (1996). In this simulation, the seed leaf azimuths are distributed as if the planter would deliver the seeds perfectly at the predicted angles of the stable points. The distribution in the histogram is still clearly identifiable as across-row.

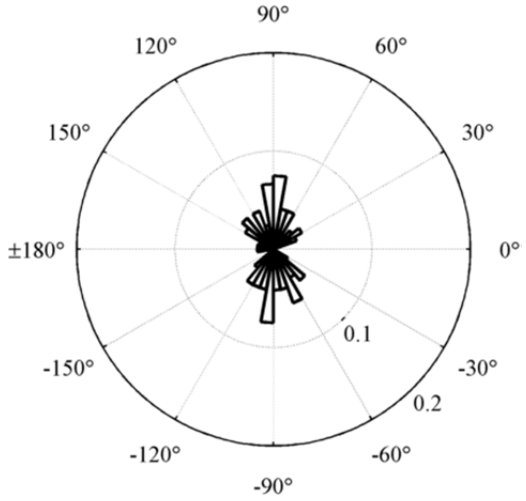

Figure 52. 120 simulated seed leaf azimuths of a hybrid DKC-6346 without considering the variability of the planter.

The “average” variability of the planter performance for this hybrid was identified in the soil bin test to adhere to a concentration parameter of about 3.2. The concentration parameters of the

seed-to-leaf models were combined with the planter variability according to Eq. 5.1 and yielded $\kappa'_1 = 2.01$ and $\kappa'_2 = 1.33$ for embryo up and down, respectively. If this variability of the planter is added to the simulated mixture, the resulting the circular histogram takes the shape as depicted in Figure 53.

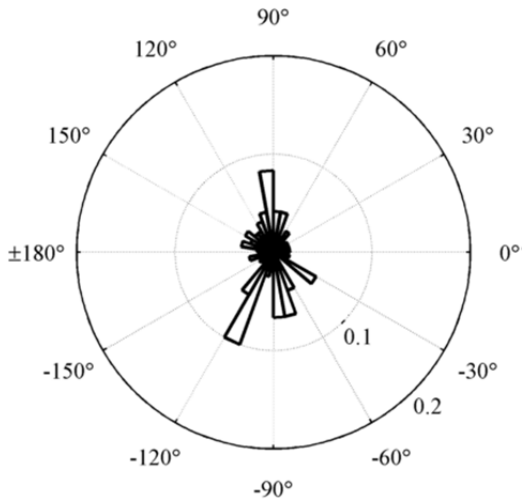

Figure 53. Histogram of 120 simulated plants with combined seed leaf variability and the planter inaccuracy.

Such a histogram resembles much more the ones obtained from the recorded field data. In fact, the V-test applied to this data set leads to the conclusion that it is different from uniformly random data only at a significance level of 0.15.

The efforts of estimating field performance based on post-emergence data are therefore in vain. The various modes are not expressed strongly enough in the data set. Alleviation may be provided by much larger sample sizes and possibly an alternative seed angle indicator. For example, measuring Leaf 1 instead of the seed leaf may provide models with higher concentration parameters and therefore more power to identify the performance parameters of the planter.

References

Drouet, J. L., and B. Moulia. 1997. Spatial re-orientation of maize leaves affected by initial plant orientation and density. *Agricultural and Forest meteorology* 88(1-4):85-100.

Drouet, J. L., B. Moulia, and R. Bonhomme. 1999. Do changes in the azimuthal distribution of maize leaves over time affect canopy light absorption? *Agronomie* 19(3-4):281-294.

Fisher, N. I. 1996. *Statistical Analysis of Circular Data*. Cambridge University Press.

Girardin, P., and M. Tollenaar. 1994. Effects of intraspecific interference on maize leaf azimuth. *Crop Science* 34(1):151-155.

Maddonni, G., M. Chelle, J. L. Drouet, and B. Andrieu. 2001. Light interception of contrasting azimuth canopies under square and rectangular plant spatial distributions: simulations and crop measurements. *Field crops research* 70(1):1-13.

Mardia, K. V., and P. E. Jupp. 2000. *Directional Statistics*. Wiley Series in Probability and Statistics. Wiley and Sons, Chichester, UK.

Torres, G., J. Vossenkemper, W. Raun, and R. Taylor. 2011. Maize (Zea Mays) Leaf Angle and Emergence as Affected by Seed Orientation at Planting. *Experimental Agriculture* 1(1):1-14.

CHAPTER V

SUMMARY AND CONCLUSION

The work discussed represents a first effort into mechanization of seed oriented planting in corn production. Although seed kernels are graded, their shapes are still far from uniform and individual handling of naturally variable seeds remains a challenge. However, if seed orientation can be introduced into commercial planting equipment, the potential direct yield benefits as well as numerous advantageous secondary effects like enhanced water and nutrient use efficiency may provide sound economic as well as ecological viability of seed orientation in commercial corn production in the near future. In the following, the key discoveries of this work are summarized and potential entry points for future work discussed.

Key Discoveries and Results in Light of the Specific Objectives

Specific Objective 1:

1. *Seed orientation may be achieved through the concept of pushing*, similarly to widely used technology for part feeding in manufacturing and assembly industries.
2. *Seed orientation performance by pushing can be predicted by computational analysis of seed shapes*. A highly simplified model based on the radius function of the polygonal convex hull of the projection of the seed shape onto the major principal plane is able to predict the interaction between the seed and an infinite, straight pushing plane. The analysis showed that the stable orientation angles of the seeds – independent on hybrid –

are the located at roughly ±80° as measured from the seed's reference line along the long axis. With the pushing plane perpendicular to the row direction, this would produce seeds that were expected to be orientation ±80° with respect to the row direction. Data collected in a bench unit showed that the forecast orientation performance inside the mechanism can be very accurately reproduced.

3. *Suitability and seed orientation performance is hybrid dependent.* This work was able to show that the kernels of the hybrids DKC-6342 and DKC-6346 possess consistently three stable angular orientations with one additional local minimum located opposite the caryopsis attachment point. Bench unit test also showed that the third, unfavorable aspect for across-row leaf azimuths was only marginally stable and would occur with much lower probability than predicted. The kernels of the hybrid P0902HR only possess two stable orientations because the pericap is quite rounded opposite the caryopsis attachment point. However, the calculated variability of the stable points for the kernels of P0902HR is larger than for than for DKC-6342 and DKC-6346. The kernels of the hybrid P1162HR proved to be not very suitable for seed orientation because their discoidal shape results in sometimes several locally weakly stable angular orientations. The hybrid DKC-6342 produced consistently the most favorable results for seed orientation throughout this work.

Specific Objective 2:

4. *Seed orientation can be integrated in a continuous process into existing planter technology*. The concept of seed orientation by pushing was designed to directly interface with existing, continuously operating seed singulation and furrow opening and closing processes. Nonetheless, the solution presented here operates at much slower speeds than commercial equipment.

5. *One of the keys to successful seed orientation is the control of the relative velocity between the seed and the ground at the time of the release.* For planter concepts of the type discussed here where the seed is first oriented and then placed in the ground, the transition of the seed from the orientation mechanism to the ground is of critical importance. It has been shown that if the velocity of the seed is less than the velocity of the ground, seed orientation is lost in the transition. In fact, the seed must be at least at velocity parity for the orientation to be maintained after the seed comes to rest in the furrow.
6. *Closing wheels on the planter appear to have no negative effect on planter performance.* The process of furrow closing appears to be better controlled and possibly more consistent if executed by closing wheels than by manual operation. The results show that the orientation performance is consistently better with closing wheels.

Specific Objective 3:

7. *Seed leaf azimuth distribution with respect to a seed's direction can be modeled by von Mises distributions.* Detailed greenhouse experiments with seeds of the four test hybrids have confirmed that the seed leaf azimuth distribution is highly non-uniform. In fact, the distribution can be very well approximated by a von Mises model. The experiments furthermore, revealed that the concentration parameter depends on whether the seeds are oriented "embryo up" or "embryo down" at the time of planning. The mean seed leaf direction lies roughly 180° opposites for the two different orientations.
8. *The seed leaf azimuth distribution for corn planted by this mechanization concept is expected to be a mixture containing four modes.* The combination of the results from Phase II and Phase III reveals that determination of planter orientation performance after the plants have emerged is difficult at best. Although models of the seed-to-leaf azimuth

distribution could be identified, the fact that seed leaves emerge at 180° offset when planted “embryo down”, the identification of planter performance parameter from the mixture is not possible because the modes are not pronounced strongly enough for the data to be separable.

Future Work

This first effort at seed orientation mechanization has also generated a lot of new questions, some which are now proposed here as entry points for future research.

1. The exterior shape of the seed suggests that a straight pushing plane may not be optimal because the seed is already oriented at a bias of roughly 10° on average across all hybrids. An improved design of the shape of the pushing edge could eliminate this source of error.
2. Observations in the bench unit have indicated that the distance over which the seeds must be push to be oriented could be drastically shortened. It could be observed that the seed would immediately start to rotate when contacting the pushing plane and then commence translation. After only a few millimeters of translational motion the seed was already oriented. This could lead to a much more compact orientation mechanism design.
3. Besides the control of r_v, the transition of the seed from the mechanism to the ground in general remains a very difficult step in the process. The design implemented for this work was directly and rigidly coupled to the frame of the planter. Therefore, the geometry of the three-point attachment needed to be adjusted very precisely in order to ensure the seed release edge on the orientation mechanism was as close to the ground as possible. An alternative mounting concept with respect the planter frame may alleviate this problem. Also, the height of the release edge for the design used in this work was only

about 3 to 4 mm. Nonetheless, this is still in the same order magnitude as the seed's dimensions. This may still be too high and introduce too much uncontrollable error.

4. The belt design was an obvious solution for an implementation of a pushing plane concept. However, it responded not too well to the inherently dusty and sandy environment in the furrow. Therefore, a simpler concept, possibly based on a wheel may warrant consideration.
5. The fact that the kernels are roughly 12 to 15 mm long and that they must be oriented across-row requires the furrow to be cut of appropriate width and flat bottom. This is considerably more work than required by state-of-the-art no-till planter systems that minimize the energy invested in groove forming by merely cutting a slit where the seed is injected. It may therefore be beneficial to investigate the feasibility of mechanizing the up-right seed orientation.
6. Lastly, the post-emergence performance measurement method must be refined. One may consider using a higher ranked leaf as a seed angle indicator. However, this leaf must still be of an early stage in the plant development such that the influence between plants is minimized. Alternatively, one may consider developing a method that allows a much faster collection of much larger data sets. The application of proper statistical methods may then produce more detailed insight.

APPENDICES

Appendix A: Control Program for the Planter Prototype

```
// CONTROLLER FOR THE SEED ORIENTATION PLANTER TESTBED
//
// 2012/07/13, ak:  pulled all "fiddling files" together into
//                  a first version
//                  - reads encoder
//                  - outputs square waves on the motor drive pins
// 2012/07/19, ak:  Got data logging onto SD card to work
//                  scale factors for relative speed control added
// 2012/07/20, ak:  Implemented a 5-point moving average filter on the encoder signal
// 2012/07/26, ak:  Implemented a 2-pole Chebychev filter on the encoder signal

#include "Arduino.h"
#include <digitalWriteFast.h>
#include <SD.h>
#include <Wire.h>
#include <RTClib.h>


// data logging on SD card
const int sdChipSelect = 10;
File logfile;
#define REDLEDPIN 3
#define GREENLEDPIN 4

// generic filename prototype.
// Does not overwrite existing filenames.
// It will increment the file idx at the end of the name.
char filename[] = "LOGGER00.CSV";


// real-time clock for data logging
RTC_DS1307 RTC;

// Quadrature encoder
// on Arduino UNO, IRQ 0 is internally connected to Pin 2!
#define encoderInterrupt 0
// Signal A is connected to Pin 2, triggering the
// interrupt on the rising edge of the encoder
#define encoderPinA 2
// Signal B of the encoder
#define encoderPinB 5
volatile bool encoderBSet;
volatile long encoderTicks = 0;
volatile long encoderTicksFilt = 0;

// loop timing, 10Hz (interval in ms)
```

```
#define LOOP_INTERVAL 100

// Stepper motors
volatile int beltTimerOverflows = 0;
volatile int beltMotorFreq = 0;
volatile int discTimerOverflows = 0;
volatile int discMotorFreq = 0;
#define TIMERFREQ 10000
#define beltMotorPin 7
#define discMotorPin 6
#define beltMotorDirPin 8
#define discMotorDirPin 9


// *** scale factor for the belt motor ***
// const float encppr = 200;
// const float encrevpwheelrev = 3.5;
// const float wheelpprev = 700;
// const float wheelcirc = 50.25; // circumference of the wheel
// const float encppinch = wheelpprev/wheelcirc; // encoder pulses per inch: 13.93
const float encpulseperinch = 13.93;
// const float stepspbeltinch = 10;
const float pulsesperbeltinch = 400/7.2;   // we're running half-steps
const float compensationFactor = 1.1; // belt speed with respect to ground speed
// const float encmeasurementspersecond = 10;
const float beltMotorScale = pulsesperbeltinch*compensationFactor/encpulseperinch*10;
//const float beltMotorScale = 14.357;


// *** scale factor for the disc motor ***
const float seedSpacing = 7.0;          // inches per seed
const float inpseed = 1/seedSpacing;     // seed per inches
// const float pulsespercell = 69.136;   // 30 cell disc
const float pulsespercell = 207.408;     // 10 cell

// factor 10 because reading encoder at 10Hz
const float discMotorScale = pulsespercell/encpulseperinch*inpseed*10;

// encoder signal filter
//#define USE_MOVINGAVERAGE_FILTER    // half-second moving average
// 2-pole Chebychev LP, 0.1 SF cut-off
//--> Smith, DSP Guide, http://www.dspguide.com, Chapter 20, p. 336
#define USE_IIRFILTER_1HZCO
// 2-pole Chebychev LP, 0.2 SF cut-off
//#define USE_IIRFILTER_2HZCO

#ifdef USE_MOVINGAVERAGE_FILTER
// temp vars for the moving average filter
  volatile long x0 = 0, x1 = 0, x2 = 0, x3 = 0, x4 = 0;
#endif // USE_MOVINGAVERAGE_FILTER

// 0.5 Hz c/o
// a0=  1.868823E-02
// a1=  3.737647E-02
// a2=  1.868823E-02
// b1=  1.593937E+00
// b2= -6.686903E-01

#ifdef USE_IIRFILTER_1HZCO
#define USE_IIR_FILTER
```

```
// filter parameters, 0.1 fs
const float a0 = 0.06372802;
const float a1 = 0.1274560;
const float a2 = 0.06372802;
const float b0 = 1.194365;
const float b1 = -0.4492774;

// measured and predicted values
float x0 = 0.0;
float x1 = 0.0;
float x2 = 0.0;
float y0 = 0.0;
float y1 = 0.0;
#endif // USE_IIRFILTER_1HZCO

#ifdef USE_IIRFILTER_2HZCO
#define USE_IIR_FILTER
// filter parameters, 0.2 fs
const float a0 = 0.1997396;
const float a1 = 0.399479201;
const float a2 = 0.1997396;
const float b0 = 0.4291048;
const float b1 = -0.2280633;

// measured and predicted values
float x0 = 0.0;
float x1 = 0.0;
float x2 = 0.0;
float y0 = 0.0;
float y1 = 0.0;
#endif // USE_IIRFILTER_2HZCO

//#define PRINT_CONSOLE

// Interrupt service routine quadrature encoder
void HandleEncoderInterrupt()
{
  // Test transition; since the interrupt will only fire on 'rising' we don't need to read pin A
  encoderBSet = digitalReadFast(encoderPinB);   // read the input pin
  // depending on direction, add or subtract a count
  encoderTicks += encoderBSet ? -1 : +1;
  // below: change addition to subtraction if encoder should turn backwards
}

// interrupt service routine to handle line toggle on motor drivers
ISR(TIMER1_COMPA_vect)          // timer compare interrupt service routine
{
  // handle the belt motor
  if( beltTimerOverflows > 0) {
    // decrement the overflow counter
    beltTimerOverflows--;
  } else {
    if( beltMotorFreq > 0 ) {
      beltTimerOverflows = (int)(TIMERFREQ/beltMotorFreq)+1;
      if( beltTimerOverflows >= TIMERFREQ/2 || beltTimerOverflows == 1) {
      // that means the motor frequency is less than 1Hz so just stop, do nothing
      } else {
        digitalWrite(beltMotorPin, digitalRead(beltMotorPin) ^ 1);   // toggle pin
      }
    }
```

```
  }

  // handle the disc motor
  if( discTimerOverflows > 0) {
    // decrement the overflow counter
    discTimerOverflows--;
  } else {
    if( discMotorFreq > 0 ) {
      discTimerOverflows = (int)(TIMERFREQ/discMotorFreq)+1;
      if( discTimerOverflows >= TIMERFREQ/2 || discTimerOverflows == 1) {
      // that means the motor frequency is less than 1Hz so just stop, do nothing
      } else {
        digitalWrite(discMotorPin, digitalRead(discMotorPin) ^ 1);   // toggle pin
      }
    }
  }
}

// initialize everything
void setup() {
  // serial terminal
  Serial.begin(115200);
  Serial.print("*****************************\n");
  Serial.print("       Planter Testbed       \n");
  Serial.print("                             \n");
  Serial.print("       (c) A. Koller         \n");
  Serial.print("         2012/07/18          \n");
  Serial.print("                             \n");
  Serial.print("                             \n");
  Serial.print("*****************************\n\n\n");

  // Quadrature encoders
  Serial.print("\nInitializing encoder...");
  pinMode(encoderPinA, INPUT);      // sets pin A as input
  pinMode(encoderPinB, INPUT);      // sets pin B as input
  attachInterrupt(encoderInterrupt, HandleEncoderInterrupt, RISING);
  Serial.print(" done.");

  // belt motor
  Serial.print("\nInitializing belt motor...");
  pinMode(beltMotorPin, OUTPUT);
  pinMode(beltMotorDirPin, OUTPUT);
  digitalWrite(beltMotorDirPin, 0);   // this motor turns "natively" in the right direction
  Serial.print(" done.");

  // disc motor
  Serial.print("\nInitializing disc motor...");
  pinMode(discMotorPin, OUTPUT);
  pinMode(discMotorDirPin, OUTPUT);
  digitalWrite(discMotorDirPin, 1);   // this motor must turn the other way
  Serial.print(" done.");

  // initialize timer1 --> this is the 16-bit timer.
  Serial.print("\nInitializing timer...");
  noInterrupts();           // disable all interrupts
  TCCR1A = 0;
  TCCR1B = 0;
  TCNT1  = 0;

  OCR1A = 800;              // this makes a 10kHz timer
```

```
  //OCR1A = 1250;          // compare match register 16MHz/256/2Hz
  TCCR1B |= (1 << WGM12);   // CTC mode
  TCCR1B |= (1 << CS10);    // no prescaling
  TIMSK1 |= (1 << OCIE1A);  // enable timer compare interrupt
  interrupts();             // enable all interrupts
  Serial.print(" done.");

  // SD card logger
  // initialize the SD card
  Serial.print("\nInitializing SD card...");
  // make sure that the default chip select pin is set to
  // output, even if you don't use it:
  pinMode(10, OUTPUT);
  pinMode(GREENLEDPIN, OUTPUT);
  pinMode(REDLEDPIN, OUTPUT);

  // see if the card is present and can be initialized:
  if (!SD.begin(sdChipSelect)) {
    Serial.println("Card failed, or not present");
    return;
  }
  Serial.println(" done.\n\n");

  // create a new file
  for (uint8_t i = 0; i < 100; i++) {
    filename[6] = i/10 + '0';
    filename[7] = i%10 + '0';
    if (! SD.exists(filename)) {
      // only open a new file if it doesn't exist
      logfile = SD.open(filename, FILE_WRITE);
      break;  // leave the loop!
    }
  }

  if (! logfile) {
    return; //error("couldnt create file");
  }

  Serial.print("Logging to: ");
  Serial.println(filename);

  // real-time oscillator
  Wire.begin();
  if (!RTC.begin()) {
    logfile.println("RTC failed");
    Serial.println("RTC failed");
  }
}

// main loop

int myinit = 1;

void loop() {
  DateTime now;

  // wait for the next loop to start
  delay((LOOP_INTERVAL -1) - (millis() % LOOP_INTERVAL));

  //digitalWrite(GREENLEDPIN, HIGH);
```

```
  logfile = SD.open(filename, FILE_WRITE);

  // write the header to file

  uint32_t m = millis();
//  if( m %1000 == 0) {
//    Serial.print("time since start: ");
//    Serial.print(m/1000);
//    Serial.print("s\n");
//  }
  logfile.print(m);           // milliseconds since start
  logfile.print(", ");

#ifdef PRINT_CONTSOLE
  Serial.print(m);         // milliseconds since start
  Serial.print(", ");
#endif

  // encoder ticks
  logfile.print(encoderTicks);
  logfile.print(", ");

#ifdef PRINT_CONSOLE
  Serial.print(encoderTicks);
  Serial.print(", ");
#endif

  // lets read the encoder
  noInterrupts();  // turn off the interrupts
  // disregard negative encoder counts
  if( encoderTicks < 0) {
    encoderTicks = 0;
  }
#ifdef USE_MOVINGAVERAGE_FILTER
// move the values in the filter vector
  x4 = x3;
  x3 = x2;
  x2 = x1;
  x1 = x0;
  x0 = encoderTicks;

  // run the moving average filter
  encoderTicksFilt = (long)((x0 + x1 + x2 + x3 + x4)/5.0);
#endif // USE_MOVINGAVERAGE_FILTER

#ifdef USE_IIR_FILTER
      // compute the filter output
      x0 = encoderTicks;
      encoderTicksFilt = (long)(a0*x0 + a1*x1 + a2*x2 + b0*y0 + b1*y1);
      if( encoderTicksFilt < 0 ) {
        encoderTicksFilt = 0;
      }
      // move the values along
      x2 = x1;
      x1 = x0;
      y1 = y0;
      y0 = encoderTicksFilt;
#endif // USE_IIRFILTER

  // motors
```

```
  // update the required frequency
  beltMotorFreq = (int)(encoderTicksFilt*beltMotorScale);
  discMotorFreq = (int)(encoderTicksFilt*discMotorScale);

  // after these calcs, reset the encoderTicks
  encoderTicks = 0;

  interrupts(); // turn the interrupts back on

  // log everything
  logfile.print(beltMotorFreq);
  logfile.print(", ");
  logfile.print(discMotorFreq);
  logfile.print("\n");
  logfile.close();  // need to close the file, otherwise data won't stick in when resetting the CPU

#ifdef PRINT_CONSOLE
  Serial.print(beltMotorFreq);
  Serial.print(", ");
  Serial.print(discMotorFreq);
  Serial.print("\n");
#endif
  //digitalWrite(GREENLEDPIN, HIGH);
}
```

Appendix B: Circular Histograms of the In-Field Seed Leaf Azimuth Measurements

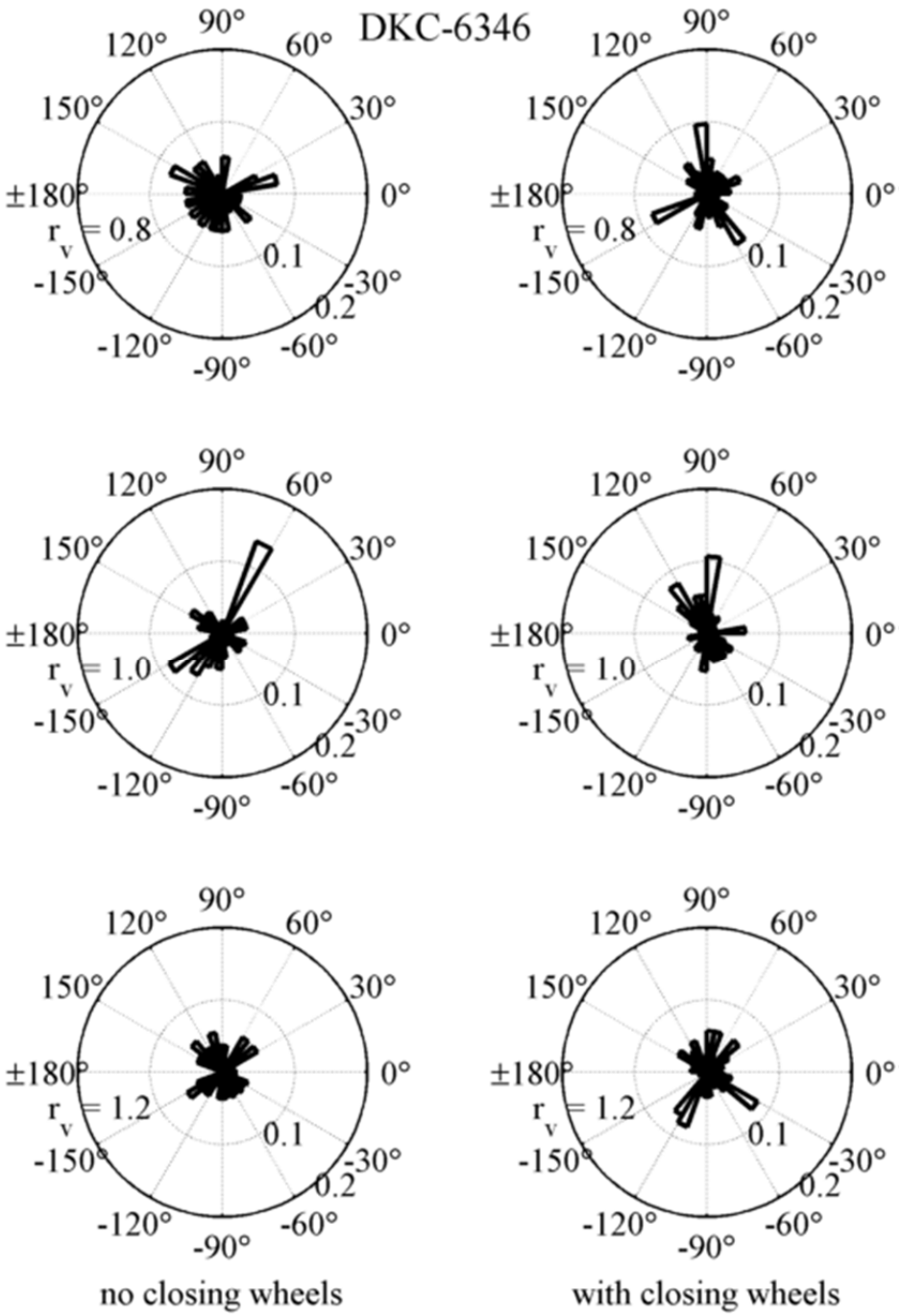

Figure 54. The circular histograms of the seed leaf azimuths for the different treatments of the hybrid DKC-6346.

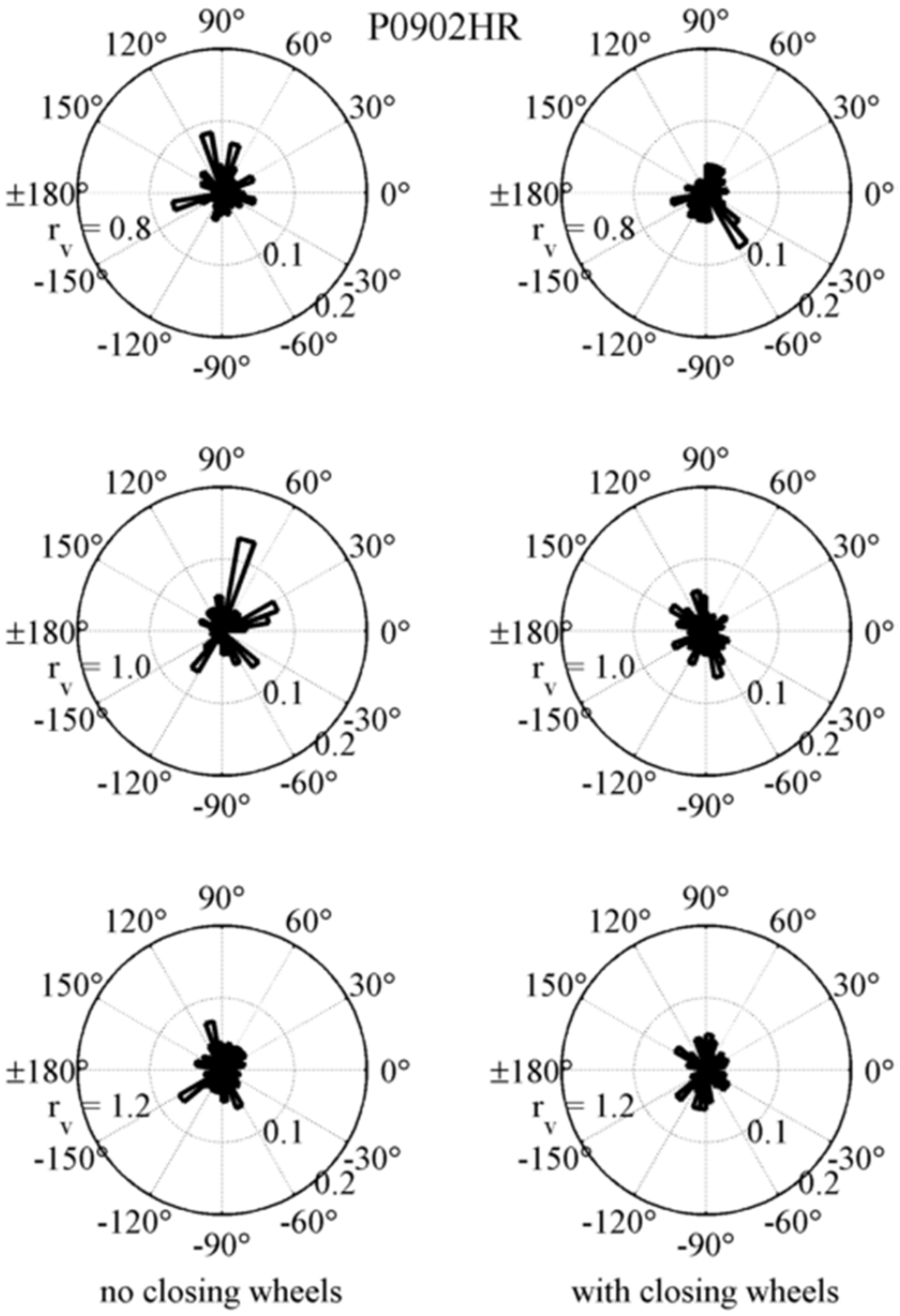

Figure 55. The circular histograms of the seed leaf azimuths for the different treatments of the hybrid P0902HR.

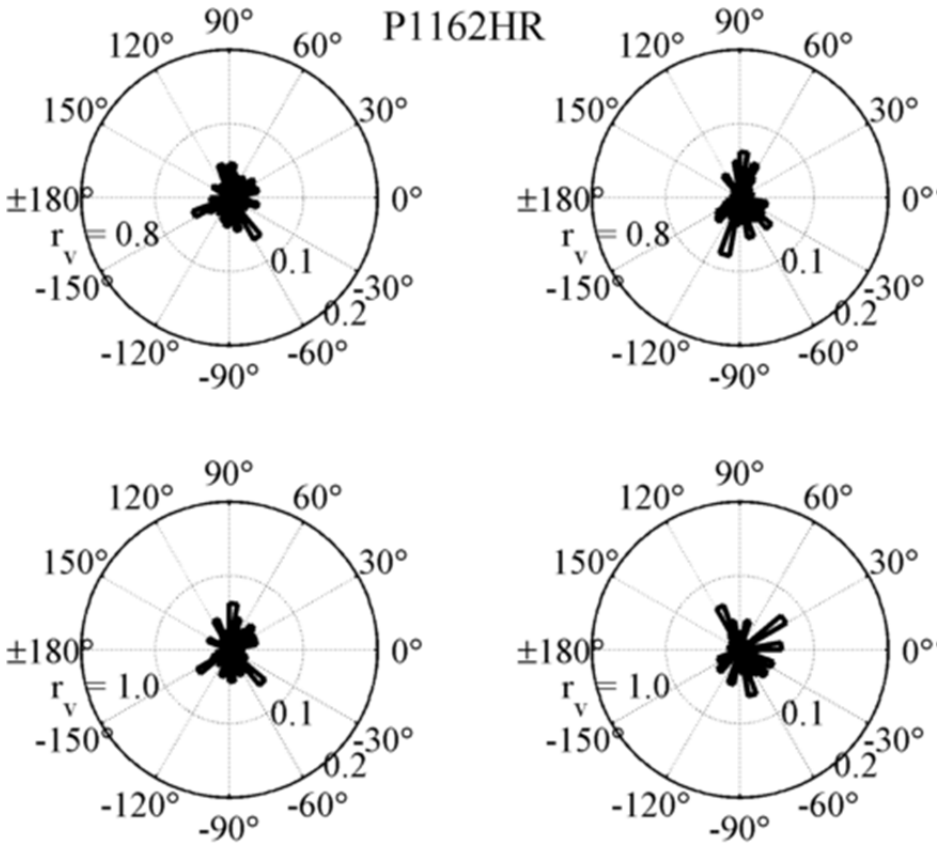

Figure 56. The circular histograms of the seed leaf azimuths for the different treatments of the hybrid P1162HR.

Appendix C: Permission for Reuse of Pictures from Service Engineering

Service Engineering picture approval Inbox x

Dennis Reynolds <Dennisr@serviceengineering.com> Feb 26

to me

Adrian,

We apologize for the late reply to your request in using our pictures for your thesis. You have our permission to use the two photographs attached to this email. Here is a little information regarding the feed systems illustrated in the pictures:

- The 10" centrifugal feeder feeds a cap at 15 parts per minute. Here is the orientation of the cap as it exits the feeder: long dimension horizontal, flat down, open end towards bowl center
- The 21" electro-polished bowl feeds an adapter at 20 parts per minute. Here is the orientation of the adapter as it exits the feeder: long dimension vertical, hanging from the flange, small end down

Again, apologies for the late response. Please feel free to contact me should you have any questions.

Thank You

Dennis Reynolds
Tech Writer
Service Engineering

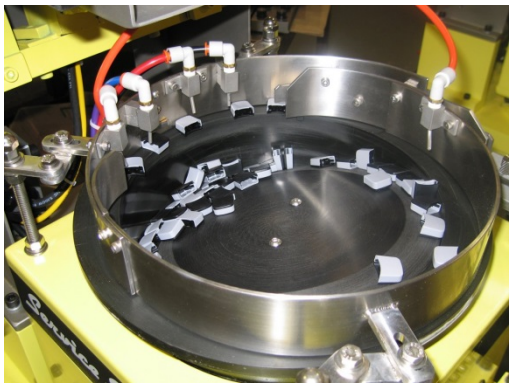

Service Engineering's 10-inch centrifugal feeder on the left and the 21-inch vibratory feeder on the right.

VITA

Adrian A. Koller

Candidate for the Degree of

Doctor of Philosophy

Thesis: DESIGN, PERFORMANCE PREDICTION AND VALIDATION OF A SEED ORIENTING CORN PLANTER

Major Field: Biosystems Engineering

Biographical:

Education:

Completed the requirements for the Doctor of Philosophy/Education in Biosystems Engineering at Oklahoma State University, Stillwater, Oklahoma in May 2013.

Completed the requirements for the Master of Science in Aerospace Engineering at Georgia Institute of Technology, Atlanta, Georgia, in May 2005.

Completed the requirements for the Bachelor of Science in Aerospace Engineering at University of Michigan in Ann Arbor, Michigan, in December 2002.

Experience:

Project Manager at Baertschi Agrartecnic AG, Switzerland since September 2012 working on specialty machinery development for agriculture.

Project Manager at RUAG Space AG in Zurich, Switzerland from 2007 until 2010 working on satellite component development involving ultra-precision mechanics, embedded controls, optics and laser.

System Engineer and Project Manager at weControl AG in Zurich, Switzerland from 2005 until 2007 working in embedded software development for unmanned aerial vehicles.

Professional Memberships:

American Society of Agricultural and Biological Engineers